RL-TR-92-332
In-House Report
December 1992

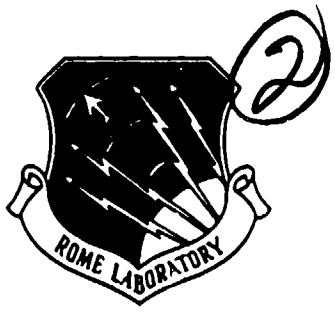

MULTICHANNEL DETECTION OF PARTIALLY CORRELATED SIGNALS IN CLUTTER

James H. Michels

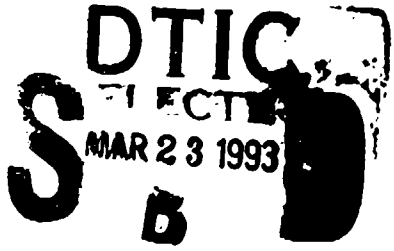

APPROVED FOR PUBLIC RELEASE; DISTRIBUTION UNLIMITED.

Rome Laboratory
Air Force Materiel Command
Griffiss Air Force Base, New York

This report has been reviewed by the Rome Laboratory Public Affairs Office (PA) and is releasable to the National Technical Information Service (NTIS). At NTIS it will be releasable to the general public, including foreign nations.

RL-TR-92-332 has been reviewed and is approved for publication.

APPROVED:

FRED J. DEMMA, Chief
Surveillance Technology Division
Surveillance & Photonics Directorate

FOR THE COMMANDER:

JAMES W. YOUNGBERG, LtCol, USAF
Deputy Director
Surveillance & Photonics Directorate

If your address has changed or if you wish to be removed from the Rome Laboratory mailing list, or if the addressee is no longer employed by your organization, please notify RL (OCTM) Griffiss AFB NY 13441-5700. This will assist us in maintaining a current mailing list.

Do not return copies of this report unless contractual obligations or notices on a specific document require that it be returned.

REPORT DOCUMENTATION PAGE

Form Approved
OMB No. 0704-0188

1. AGENCY USE ONLY (Leave Blank)	2. REPORT DATE	3. REPORT TYPE AND DATES COVERED
	December 1992	In-House Nov 91 - Oct 92

4. TITLE AND SUBTITLE
MULTICHANNEL DETECTION OF PARTIALLY CORRELATED SIGNALS IN CLUTTER

5. FUNDING NUMBERS
PE - 62702F
PR - 4506
TA - 17
WU - 67

6. AUTHOR(S)
James H. Michels

7. PERFORMING ORGANIZATION NAME(S) AND ADDRESS(ES)
Rome Laboratory (OCTM)
26 Electronic Parkway
Griffiss AFB NY 13441-4514

8. PERFORMING ORGANIZATION REPORT NUMBER
RL-TR-92-332

9. SPONSORING/MONITORING AGENCY NAME(S) AND ADDRESS(ES)
Rome Laboratory (OCTM)
26 Electronic Parkway
Griffiss AFB NY 13441-4514

10. SPONSORING/MONITORING AGENCY REPORT NUMBER

11. SUPPLEMENTARY NOTES
Rome Laboratory Project Engineer: James H. Michels/OCTM (315) 330-4431

12a. DISTRIBUTION/AVAILABILITY STATEMENT
Approved for public release; distribution unlimited.

12b. DISTRIBUTION CODE

13. ABSTRACT (Maximum 200 words)

This report considers the Gaussian multichannel binary detection problem in which the signal and non-white clutter noise are Gaussian vector processes with unknown statistics. A generalized likelihood ratio using multichannel innovations processes is implemented via a model-based approach where the signal and clutter are assumed to be characterized by autoregressive vector processes with arbitrary temporal and cross-channel correlation. The innovations processes are obtained through linear estimation using multichannel parameter estimates. Detection performance is considered as the estimates approach "steady-state" with increasing data block sample sizes. Results for two-channel signal and clutter noise vectors with various temporal and cross-channel correlation are obtained using a Monte-Carlo procedure. In the "transient-state" (estimation with limited data), the detection results are considered as a function of the data batch sizes used in parameter estimation. Furthermore, it is noted that the detection performance in the "transient-state" is related to that of the estimator which, in turn, has its own dependence upon process correlation. The results provide insight regarding the factors which control the processing time requirements to achieve a specified level of detection performance.

14. SUBJECT TERMS
Detection, Multichannel Processes, Estimation, Model-Based Detection, Innovations

15. NUMBER OF PAGES
56

16. PRICE CODE

17. SECURITY CLASSIFICATION OF REPORT	18. SECURITY CLASSIFICATION OF THIS PAGE	19. SECURITY CLASSIFICATION OF ABSTRACT	20. LIMITATION OF ABSTRACT
UNCLASSIFIED	UNCLASSIFIED	UNCLASSIFIED	U/L

ACKNOWLEDGEMENTS

The author wishes to thank Drs. P. Varshney and D. Weiner from Syracuse University for helpful comments. Special thanks to R. Vienneau from Kaman Sciences Inc. for the software engineering support.

CONTENTS

LIST OF TABLES

LIST OF FIGURES

$P_{fa}=6.93x10^{-4}$, $(S/N)_1=(S/N)_2=-5dB$, $N_T=10$, J=2, channel j signal temporal correlation parameter $\lambda_{s_{jj}}$ and signal cross-correlation parameter ρ_s.

10 Probability of detection versus (S/N) for a Gaussian signal in additive Gaussian clutter plus white noise; $P_{fa}=6.93x10^{-2}$, $(S/N)=(S/N)_1=(S/N)_2$, J=2, $N_T=10$, channel j signal and clutter temporal correlation parameters $\lambda_{s_{jj}}$ and $\lambda_{c_{jj}}$, signal and clutter cross-correlation parameters ρ_s and ρ_c, respectively.

11 Probability of detection versus (S/N) for a Gaussian signal in additive Gaussian clutter plus white noise; $P_{fa}=6.93x10^{-4}$, $(S/N)=(S/N)_1=(S/N)_2$, J=2, $N_T=10$, channel j signal and clutter temporal correlation parameters $\lambda_{s_{jj}}$ and $\lambda_{c_{jj}}$ signal and clutter cross-correlation parameters ρ_s and ρ_c, respectively.

12 Probability of detection versus the number of block samples N_{TC} used in parameter estimation via the Strand-Nuttall algorithm for a Gaussian signal in additive Gaussian clutter plus white noise; $P_{fa}=6.93x10^{-2}$, $(S/N)_1=(S/N)_2=-5dB$, $N_T=10$, J=2, channel j signal and clutter temporal correlation parameters $\lambda_{s_{jj}}$ and $\lambda_{c_{jj}}$, signal and clutter cross-correlation parameters ρ_s and ρ_c, respectively.

13 Probability of detection versus the number of block samples N_{TC} used in parameter estimation via the Strand-Nuttall algorithm for a Gaussian signal in additive Gaussian clutter plus white noise; $P_{fa}=6.93x10^{-4}$, $N_T=10$, J=2, channel j signal and clutter temporal correlation parameters $\lambda_{s_{jj}}$ and $\lambda_{c_{jj}}$, signal and clutter cross-correlation parameters ρ_s and ρ_c, respectively.

14 Probability of detection versus the number of block samples N_{TC} used in parameter estimation via the Strand-Nuttall algorithm for a Gaussian signal in additive Gaussian clutter plus white noise; J=2, $N_T=10$, channel j signal and clutter temporal correlation parameters $\lambda_{s_{jj}}$ and $\lambda_{c_{jj}}$, signal and clutter cross-correlation parameters ρ_s and ρ_c, respectively.

CHAPTER 1 INTRODUCTION

Model-based parametric approaches for detection of time-correlated signals in non-white Gaussian noise have been given considerable attention. The utilization of these methods for radar applications has been considered in [1-6]. An important feature of the model-based methods is their ability to utilize modern parameter estimators in the signal processing. In this scheme, the processes are whitened through a causal transformation of the observation data [1] using prediction error filters. Implementation architectures utilize either recursive or block processing methods to determine the weights in prediction error filtering methods [3,5]. An extension of these procedures to multichannel vector processes has recently been addressed [7]. In [7], a multichannel generalized likelihood ratio was derived using the conditional covariance matrix of the complex vector observation processes given past and present data. It was implemented using the model-based approach where the signal and the non-white noise (clutter) vector processes are assumed to be characterized by the output of a linear system driven by a white Gaussian noise vector. Furthermore, the derivation made no assumption of statistical independence between the signal and clutter processes and is thus expected to retain robustness in the presence of multipath (or reverberation) for applications in radar and sonar problems.

The use of multiple channels provides additional information and results in better performance than the single channel case. The additional information is extracted by removing the redundant (i.e. correlated) information from the observation data. This is achieved via estimation methods which "whiten" the data in time and space (i.e., across channels). The resulting uncorrelated error processes are the 'innovations' and contain in a compact form all the useful or 'new' information about the processes. In this analysis, they are utilized to determine a sufficient statistic for the hypothesis testing.

Application areas include signal detection, estimation and discrimination for radar, sonar, biomedical and geophysical problems. For radar problems, the model-based multichannel approach establishes a framework for the consideration of sensor systems using multi-frequencies and/or polarization diversity, the centralized processing of netted sensor suites and the processing of diverse, yet correlated, processes. In biomedical research, the procedure may be applied to the processing of signals such as multiple EEG brain waves for seizure state detection and classification.

This report considers the Gaussian multichannel binary detection problem in which the desired signal is random, the additive clutter disturbance is non-white, and both processes have 'unknown' statistics. In the model-based approach considered here, the signal and clutter are characterized by autoregressive (AR) vector processes. In this case, the parameters of the underlying processes are 'unknown' and must be estimated from the observation data. Detection performance is presented using a Monte-Carlo procedure as the estimators approach their steady-state values (ie., when the time sample window sizes in the estimation procedure are sufficient to obtain near optimai performance). These results provide a determination of the detection performance as a function of the algorithm convergence rates. Furthermore, these convergence rates are considered as a function of both signal and clutter-to-noise ratios as well as the temporal and cross-channel correlation properties associated with the signal and clutter processes. These results provide insight as to the processing time requirements associated with the estimators under various conditions of channel diversity as well as signal and clutter power levels.

For the steady-state case, detection results have been obtained [7] and validated with available detection curves [10] for the extreme cases of signal temporal correlation as described by Swerling case I and II targets. The results presented in this report are shown to converge to these values in the limit of large data. Detection results are also considered for the case of unequal signal-to-noise ratios on each channel thus revealing the impact of a degraded channel on overall performance. Finally, in these detection computations, observation vector processes are synthesized using a multichannel time series method [8,9] capable of providing parametric variations in temporal and spatial (ie., cross-channel) correlation as well as in the signal-to-noise (S/N) and clutter-to-noise (C/N) ratios. As such, the signal generation method used in this investigation provides target models which lie between the bounds of the Swerling temporal fluctuation models as well as for varying degress of cross-channel correlation.

In chapter 2, the detection problem is presented along with a description of the partially correlated signal models. Chapter 3 contains a derivation of the multichannel likelihood ratio used to compute the detection results. The content of these two sections has been described in [7,16] and is presented here for completeness. Implementation architectures for the computation of the sufficient statistic are shown in chapter 4 with Monte-Carlo results presented in chapter 5. A discussion and summary of the results are contained in chapters 6 and 7,

respectively. Finally, an abbreviated version of this report has been presented in [17].

CHAPTER 2 THE DETECTION PROBLEM

In this chapter, we discuss the multichannel detection problem addressed in this report. In addition, the models of the random signal and clutter processes are also described. The multichannel binary detection problem is expressed as

$$H_1: \quad \underline{x}(n) = \underline{s}(n) + \underline{c}(n) + \underline{w}(n) \qquad n = 1,2,...,N \qquad (1a)$$

$$H_0: \quad \underline{x}(n) = \underline{c}(n) + \underline{w}(n) \qquad n = 1,2,...,N, \qquad (1b)$$

where the discrete received observation process $\underline{x}(n)$ is a zero mean, wide-sense jointly stationary Jx1 baseband vector consisting of J channels. The vectors $\underline{s}(n)$, $\underline{c}(n)$ and $\underline{w}(n)$ are zero mean, complex Gaussian random Jx1 vector processes describing the signal, non-white noise(clutter) and white noise, respectively. H_1 and H_0 denote the hypotheses under which the signal is present or absent, respectively. The vector processes $\underline{s}(n)$ and $\underline{c}(n)$ individually contain an arbitrary correlation in time and between channels. In addition, correlation is allowed between $\underline{s}(n)$ and $\underline{c}(n)$. Finally, the vector $\underline{w}(n)$ is uncorrelated with itself in time, but not necessarily across channels.

In this study, we compute detection results using a process synthesis method described in [8,9] to generate time samples of $\underline{s}(n)$, $\underline{c}(n)$, and $\underline{w}(n)$. In [7], we discuss the relationship between these synthesized processes and those denoted in the radar literature as the Swerling models for which analytical detection performance curves are available [10]. For two extremes of temporal and cross-channel correlation, these latter models are used here to provide bounds on the detection results. We designate model I(INCOH) as the signal model where all the bandpass signal amplitudes in a pulse train of N_T pulses are equal but vary randomly from pulse-train to pulse-train according to a Rayleigh distribution and the initial phase of each pulse is a statistically independent, uniformly distributed random variable. This model is used to describe the case where the phases of the echo returns are randomized due to phase instabilities associated with the transmitted waveform. We designate model II(INCOH) as the signal model where both the amplitudes and phases of the echo pulses are statistically independent random variables with Rayleigh and uniform distributions, respectively. Models I(INCOH) and model II(INCOH) provide the two extremes on the amplitude correlation of the processes. For a coherent transmitted pulse train, we define

model I(COH) as the signal model where the amplitudes over each entire pulse train are totally correlated random variables as are the initial phases. However, they are uncorrelated between pulse trains with Rayleigh and uniform distributions, respectively. In [7], these models are generalized for the multichannel case.

In [8,9], autoregressive processes $AR(p_g)$ of order p_g are synthesized individually for the signal (g=s) and clutter (g=c). The temporal correlation of the jth channel is controlled by the one-lag temporal correlation parameter, λ_{jj}. For low temporal correlation, $\lambda_{jj} \rightarrow 0$; for high temporal correlation, $\lambda_{jj} \rightarrow 1$. Likewise, the cross-channel correlation is controlled by the one-lag temporal cross-correlation parameter λ_{ij} (which relates to the width of the cross-correlation function) and by the cross-channel correlation parameter $|\rho_{ij}|$ where $\rho_{ij}=R_{ij}(0)/\sigma_{ii}\sigma_{jj}$ and $R_{ij}(0)$ is the cross-correlation function at lag zero. Two extreme cases occur when $\lambda_{jj} \approx |\rho_{ij}| \approx 0$ and $\lambda_{jj} \approx |\rho_{ij}| \approx 1$ for all i,j=1,2,...,J. In the former case, all of the J channel processes are uncorrelated both in time and space (ie., across channels). In the latter, they are highly correlated in both of these dimensions. These two cases of synthesized processes characterize the multichannel model II(INCOH) and model I(COH) signals, respectively. Thus, the detection results computed in this report are bounded by the analytical detection curves associated with these models.

Finally, we point out that for certain applications such as radar and sonar systems, a distinct Doppler center frequency may be obtained on each of the J channels due to the operational characteristics of the multichannel system. This may result for example when each channel contains data received using a separate transmitter frequency. The result of this situation is the introduction of a non-stationarity in the covariance matrices of the multichannel processes. In this case, it may be necessary to pre-process the observation data to normalize the Doppler frequencies on each channel to that of a selected reference channel. This pre-processing procedure is discussed in [7,9] and is assumed to have been implemented for the results presented in this analysis.

CHAPTER 3 THE MULTICHANNEL LIKELIHOOD RATIO

In this chapter, we briefly present the derivation of a multichannel likelihood ratio for the detection problem of eqs(1). The derivation is described more thoroughly in [7]. First, we define the concatenated vector consisting of N time samples of the vector $\underline{x}(n)$ as

$$\underline{\underline{x}}^T_{1,N} = [\underline{x}^T(1)\ \underline{x}^T(2)...\underline{x}^T(N)]$$

where

$$\underline{x}^T(k) = [x_1(k)\ x_2(k)...x_J(k)] \qquad k = 1, 2, ..., N$$

and

$$\underline{\underline{x}}_{1,1} = \underline{x}(1).$$

Under hypothesis H_i i=0,1, the multivariate joint Gaussian density can be written as the product of conditional densities so that

$$p_X(\underline{\underline{x}}_{1,N}|H_i) = p[\underline{x}(1)|H_i] \prod_{n=2}^{N} p[\underline{x}(n)|\underline{\underline{x}}_{1,n-1},H_i] \qquad i=0,1 \tag{2}$$

and all the conditional densities are complex Gaussian. Let $\hat{\underline{x}}(n|n-1,H_i)$ denote the conditional expectation of $\underline{x}(n)$ given $\underline{\underline{x}}_{1,n-1}$ with multivariate conditional density $p[\underline{x}(n)|\underline{\underline{x}}_{1,n-1},H_i]$. Then, $\hat{\underline{x}}(n|n-1,H_i)$ is the linear minimum mean-squared error (MMSE) predictor of $\underline{x}(n)$ using past data $\underline{\underline{x}}_{1,n-1}$ assuming H_i is true. The JxJ covariance matrix of this density function is the conditional covariance matrix $K_X(n|n-1,H_i)$ such that

$$K_X(n|n-1,H_i) = E\{[\underline{x}(n) - \hat{\underline{x}}(n|n-1,H_i)][\underline{x}(n) - \hat{\underline{x}}(n|n-1,H_i)]^H\} \tag{3a}$$

$$= E[\underline{\varepsilon}(n|H_i)\underline{\varepsilon}^H(n|H_i)] \qquad n = 1,2,...,N \qquad i = 0,1 \tag{3b}$$

where

$$\hat{\underline{x}}(1|0,H_i) = \underline{0} \qquad i = 0,1 \tag{4}$$

due to the zero-mean assumption on $\underline{x}(n)$ and

$$\underline{\varepsilon}(n|H_i) = \underline{x}(n) - \underline{\hat{x}}(n|n-1,H_i) \qquad i = 0,1 \tag{5}$$

is the zero-mean MMSE vector. Assuming joint wide-sense stationarity on the narrowband bandpass processes, the conditional density functions can be expressed as [7]

$$p[\underline{x}(n)|\underline{x}_{1,n-1},H_i] =$$

$$= \frac{1}{(\pi)^J|K_X(n|n-1,H_i)|}\exp\{-[\underline{x}(n)-\underline{\hat{x}}(n|n-1,H_i)]^H[K_X(n|n-1,H_i)]^{-1}[\underline{x}(n)-\underline{\hat{x}}(n|n-1,H_i)]\}$$

$$i = 0,1. \tag{6a}$$

$$= \frac{1}{(\pi)^J|K_X(n|n-1,H_i)|}\exp\{-\underline{\varepsilon}^H(n|H_i)[K_X(n|n-1,H_i)]^{-1}\underline{\varepsilon}(n|H_i)\} \quad i = 0,1 \tag{6b}$$

where

$$p[\underline{x}(1)|H_i] = p[\underline{\varepsilon}(1)|H_i]$$

$$= \frac{1}{(\pi)^J|K_X(1|0,H_i)|}\exp\{-\underline{\varepsilon}^H(1|H_i)[K_X(1|H_i)]^{-1}\underline{\varepsilon}(1|H_i)\} \qquad i = 0,1. \tag{7}$$

Using eqs(2), (6b) and (7), the log-likelihood ratio for the multivariate joint Gaussian density function now becomes

$$\ln\Lambda_{H_1,H_0} = \ln\frac{p_X(\underline{x}_{1,N}|H_1)}{p_X(\underline{x}_{1,N}|H_0)} \tag{8a}$$

$$= \ln\frac{(p[\underline{x}(1)|H_1]\prod_{n=2}^{N}p[\underline{x}(n)|\underline{x}_{1,n-1},H_1])}{(p[\underline{x}(1)|H_0]\prod_{n=2}^{N}p[\underline{x}(n)|\underline{x}_{1,n-1},H_0])} \tag{8b}$$

$$= \ln\left[\frac{\prod_{n=1}^{N} |K_x(n|n\text{-}1,H_0)| \exp\{-\underline{\varepsilon}^H(n|H_1)[K_x(n|n\text{-}1,H_1)]^{-1}\underline{\varepsilon}(n|H_1)\}}{\prod_{n=1}^{N} |K_x(n|n\text{-}1,H_1)| \exp\{-\underline{\varepsilon}^H(n|H_0)[K_x(n|n\text{-}1,H_0)]^{-1}\underline{\varepsilon}(n|H_0)\}}\right] \tag{8c}$$

$$= \sum_{n=1}^{N}\left[\ln\frac{|K_x(n|n\text{-}1,H_0)|}{|K_x(n|n\text{-}1,H_1)|} + \underline{\varepsilon}^H(n|H_0)[K_x(n|n\text{-}1,H_0)]^{-1}\underline{\varepsilon}(n|H_0) - \underline{\varepsilon}^H(n|H_1)[K_x(n|n\text{-}1,H_1)]^{-1}\underline{\varepsilon}(n|H_1)\right]. \tag{8d}$$

Eq(8d) can be simpified further by a diagonalization of the conditional covariance matrices and an orthogonal transformation of $\underline{\varepsilon}(n|H_i)$ i=0,1 across channels. Since these matrices are Hermitian and positive semi-definite, various decompositions are possible. In [7], the LDL^H and Cholesky CC^H decompositions are considered. The resulting likelihood ratios are shown to be

$$\ln\Lambda_{H_1,H_0} = \sum_{j=1}^{J}\sum_{n=1}^{N}\left\{\ln\frac{\sigma^2_{\gamma_j}(n|H_0)}{\sigma^2_{\gamma_j}(n|H_1)} + \frac{|\gamma_j(n|H_0)|^2}{\sigma^2_{\gamma_j}(n|H_0)} - \frac{|\gamma_j(n|H_1)|^2}{\sigma^2_{\gamma_j}(n|H_1)}\right\} \tag{9}$$

and

$$\ln\Lambda_{H_1,H_0} = \sum_{j=1}^{J}\sum_{n=1}^{N}\left\{\ln\frac{|c_{\alpha_{jj}}(n|H_0)|^2}{|c_{\alpha_{jj}}(n|H_1)|^2} + |\alpha_j(n|H_0)|^2 - |\alpha_j(n|H_1)|^2\right\} \tag{10}$$

respectively. The quantities $\gamma_j(n|H_i)$ and $\alpha_j(n|H_i)$ i=0,1 are the jth channel error vectors or innovations processes which are whitened both in time and across channels under hypothesis H_i. The quantity $\sigma^2_{\gamma_j}(n|H_i)$ is the error variance for $\gamma_j(n|H_i)$ while the coefficients $c_{\alpha_{jj}}(n|H_i)$ are contained along the diagonal of the Cholesky matrix C and are related by [7]

$$\sum_{j=1}^{J} \ln \frac{\sigma^2_{\gamma_j}(n|H_0)}{\sigma^2_{\gamma_j}(n|H_1)} = \sum_{j=1}^{J} \ln \frac{|c_{\alpha_{jj}}(n|H_0)|^2}{|c_{\alpha_{jj}}(n|H_1)|^2} \qquad i = 0,1. \qquad (11)$$

CHAPTER 4 IMPLEMENTATION PROCEDURES

A block diagram of the architectures used to compute the likelihood ratios of eqs(9) and (10) are shown in Figs. 1 and 2, respectively. Fig. 1 is the multichannel extension of the implementation reported in [3,5]. The lower branch is used to compute the second term and the numerator of the first term in eq(9), while the upper branch determines the third term and the denominator of the first term. Analogous comments apply to Fig. 2. The quantity Y_b is the threshold for the decision procedure. We note that the specific choice of the prediction error filter structure will depend on the assumed underlying model of the observation processes [7]. A multichannel forward prediction error filter with a tapped delay line architecture is utilized in this investigation and is shown in Fig. 3. For this filter structure, the JxJ matrix tap weights are the forward linear prediction coefficients [13,14]. In this analysis, these coefficients are estimated directly from the observation data $\underline{x}(n)$ using the procedure described below in subsection 4c.

We now briefly describe three conditions pertaining to the use of 'a priori' information regarding the statistics of the processes (for each of the hypotheses) that is used in the estimation procedure.

4a. Known Covariance Matrix

In [7], we discuss filtering methods using multichannel linear prediction to obtain $\underline{\gamma}(n|H_i)$ and $\underline{\alpha}(n|H_i)$. For a known covariance matrix under each of the two hypotheses, two sets of filter coefficients and error variances can be obtained exactly. In this case, $\underline{\gamma}(n|H_i)$ and $\underline{\alpha}(n|H_i)$ will be minimum mean squared error (MMSE) residuals at the output of a multichannel prediction error filter (such as that shown in Fig.3) designated under hypothesis H_i. It is this case that is approached as the estimators reach steady-state.

4b. Unknown Covariance Matrix

For the unknown covariance matrix case, the filter coefficients, their order and the error variances must be estimated. Thus, eqs(9) and (10) become suboptimal generalized likelihood ratios. In practice, only one set of observation data may be available to estimate the parameters (ie., the filter coefficients and error variances) for each filter assuming the appropriate hypothesis is true. In the practical implementation for this case, we must assume that the MMSE filters

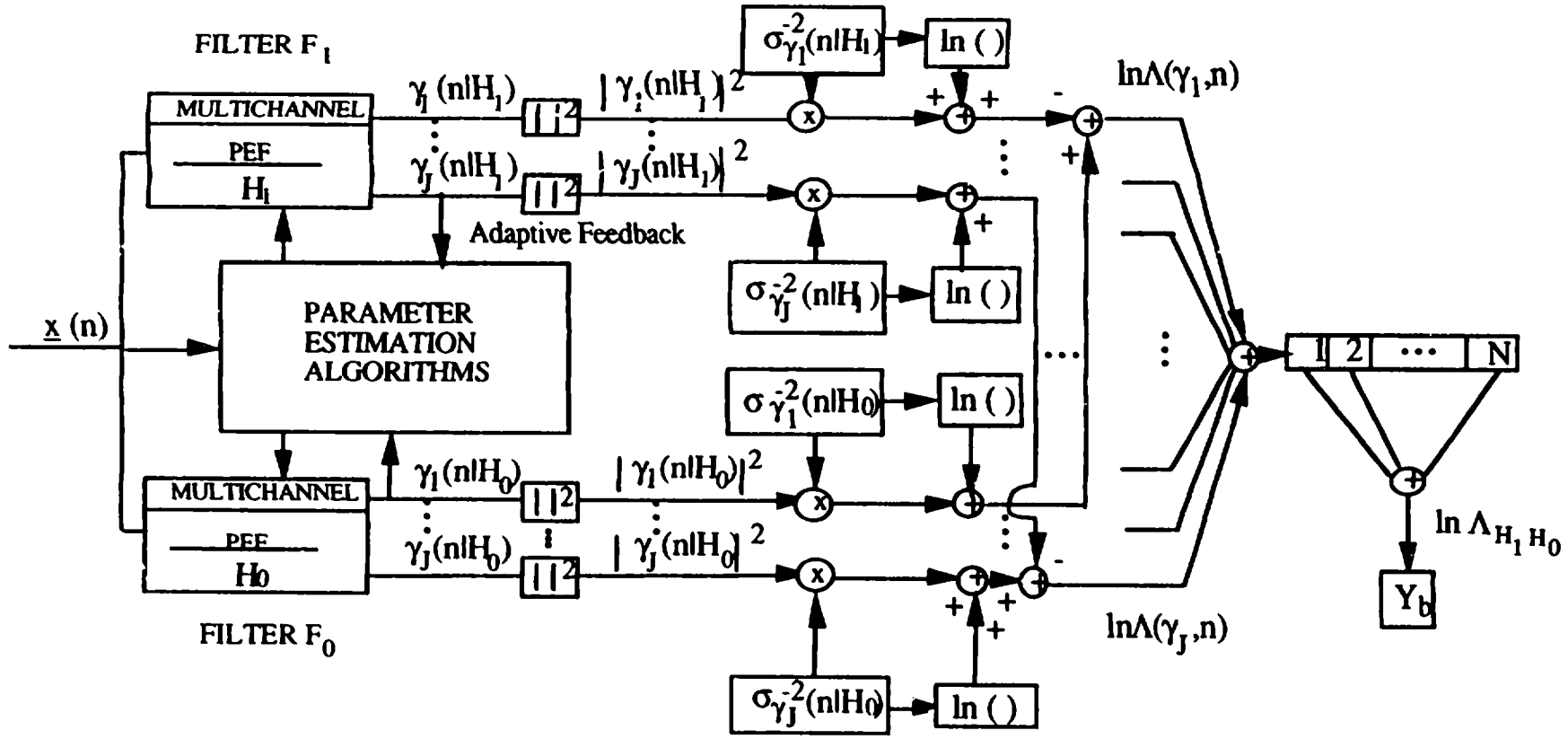

Fig. 1 Multichannel Likelihood Ratio Implementation for eq(9)

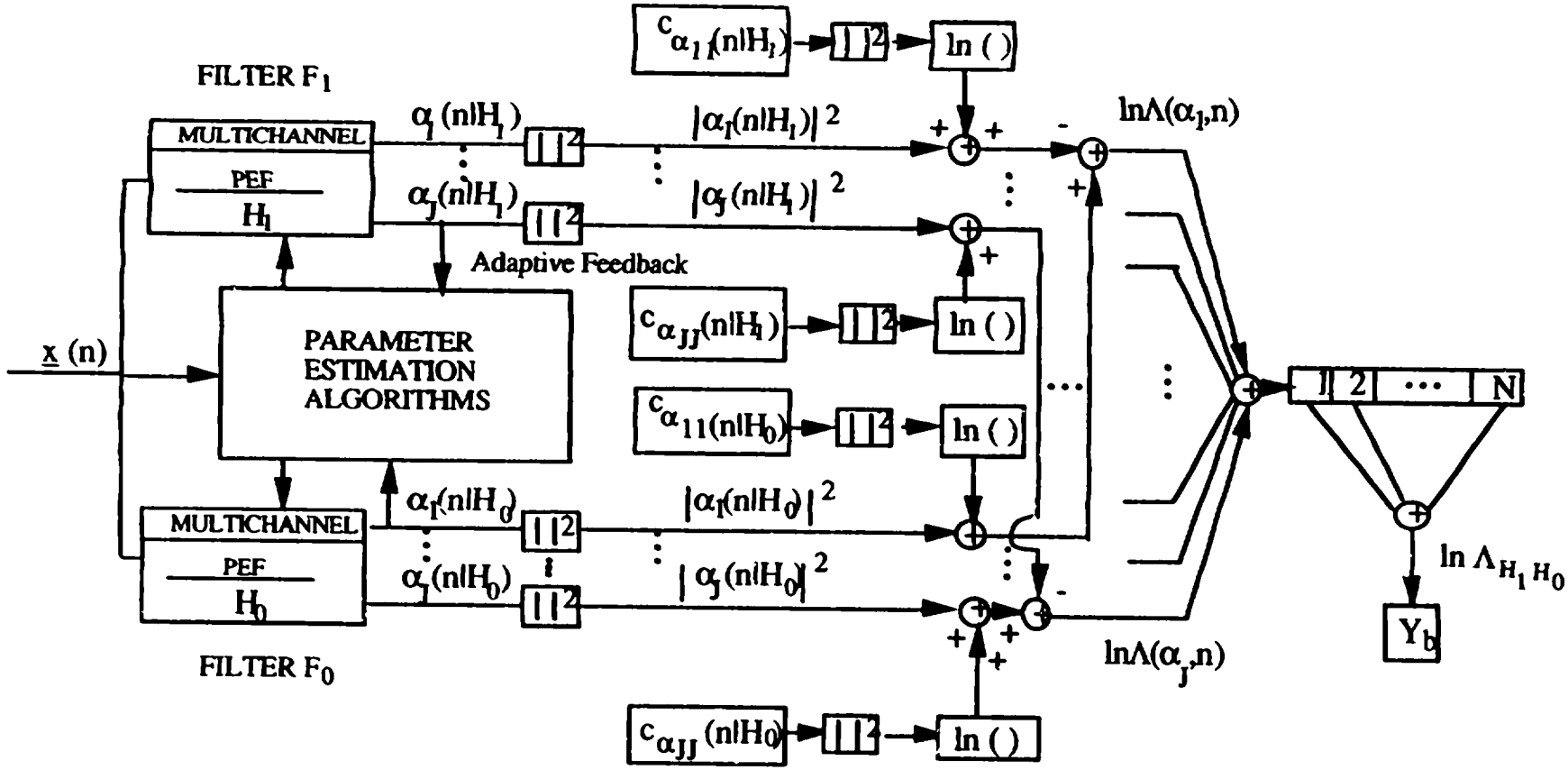

Fig. 2 Multichannel Likelihood Ratio Implementation for eq(10)

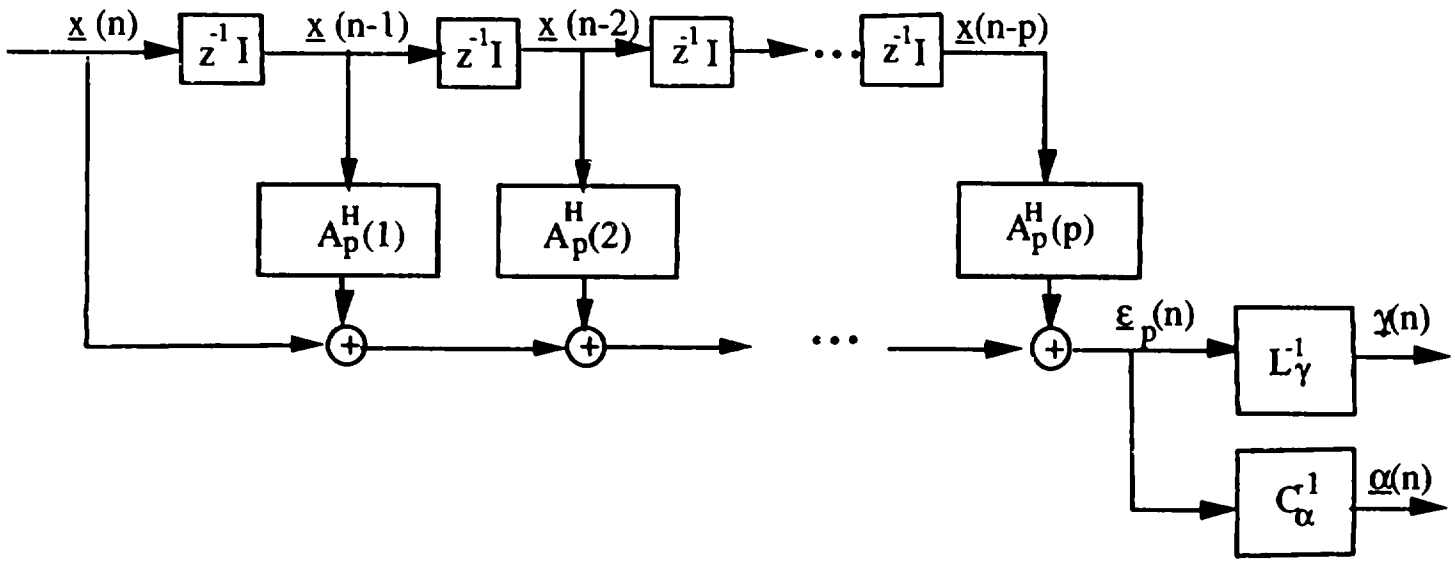

Figure 3 Multichannel Prediction Error Filter (Tapped Delay Line Structure)

under each hypothesis have unequal orders so that the likelihood ratio will, in general, have a value other than zero. This assumption is justified, for example, when characterizing the underlying signal and clutter as autoregressive processes. We note that the summation of AR processes and white noise is, in general, an autoregressive moving-average (ARMA) process which can be approximated by a higher order AR model. Thus, the order of the observation process under hypothesis H_1(signal present) is larger than that under H_0 (signal absent). Therefore, a higher order prediction error filter is used for filter F_1 than for F_0 in the practical implementation architectures for the likelihood ratios. For single channel processes, these considerations have been treated in [5].

4c. Use of 'A Priori' Data

In some applications, 'a priori' information can be used to predetermine the filter orders, the error variances and the filter coefficients [4]. In this case, data from a 'reference channel' is used to assess the hypothesis H_0 condition while data from a 'test cell' is used for that of H_1. Under these conditions, the two data sets are used to estimate the coefficients for filters F_0 and F_1, respectively. In radar applications, the 'reference channel' data is often collected from adjacent resolution cells either in azimuth or range.

In this analysis, the filter coefficients are estimated with the Strand-Nuttall algorithm [11,12] using the software routine from [13]. This algorithm is the multichannel generalization of the Burg algorithm [14]. Since this algorithm utilizes a block of data in the estimation procedure, 'a priori' data consisting of N_{TC} time samples per block are used. In some cases, coefficient averaging is performed over N_{RC} statistically independent block realizations and are assumed to be collected from the 'reference cell' data. With the filter weights fixed, the detection results are then computed using N_T time samples per channel and N_R Monte-Carlo realizations.

CHAPTER 5 DETECTION RESULTS USING MONTE-CARLO SIMULATION

In this chapter, Monte-Carlo simulation results are presented using the likelihood ratio described in eq(10) while comments on these results are deferred until chapter 6. Details of the Monte-Carlo procedure are described in [7]. The input observation data processes are generated using the process synthesis procedure described in [8,9]. Detection performance results are determined as a function of the channel signal-to-noise $(S/N)_j$ and clutter-to-noise $(C/N)_j$ ratios, the temporal and cross-channel correlation of the processes and the time sample window block sizes used to estimate the process parameters.

Two-channel (J=2) complex baseband Gaussian signal and clutter vectors were synthesized as autoregressive AR(2) processes and added to a complex Gaussian white noise vector. These observation data processes are used as an input to the system architecture shown in Fig. 2 for eq(10). In this investigation, the parameter estimators utilize 'a priori' data consisting of N_{TC} time samples per block and averaging over N_{RC} independent block realizations to estimate the filter weights as discussed in section 4c. All the detection results presented here were computed using a probability of false alarm level of 6.93×10^{-4}. The order of the F_1 and F_0 filters used in this analysis was fixed 'a priori' at eight and four, respectively. Empirical investigations have indicated insignificant performance improvement beyond these orders for the processes considered here. With the filter weights fixed, the detection results were computed via Monte-Carlo using N_R=20,000 realizations and N_T=10 time samples per channel. In [7], we considered the special case of the signal in additive white noise detection problem. Detection results were determined for N_T pulses while parameter estimation was performed using N_{TC}=10,000 time samples per block and coefficient averaging over N_{RC}=100 data blocks. Processing over these large data samples was performed in order to consider detection performance for the case where the parameter estimates have converged to their steady-state values. Selected results from [7] are shown here for the parameters listed in Table 1 with the simulated detection results plotted in Figs. 4 and 5. Equal signal-to-noise $(S/N)_j$ ratios were used on each channel at values of 3dB and -5dB. Sample standard deviations associated with the Monte-Carlo method for these simulated detection results are reported in [7]. We also plot the analytical probability of detection curves from [10] for the model I(INCOH), model I(COH) and model II(INCOH) signals using

case	λ_{11}	λ_{22}	$\lvert\rho_{12}\rvert$	$(S/N)_1$	$(S/N)_2$
1 a,b,c	0.1	0.1	0,0.5,0.99	-5dB	-5dB
2 a,b,c	0.9	0.9	0,0.5,0.99	-5dB	-5dB
3 a,b,c	0.1	0.1	0,0.5,0.99	+3dB	+3dB
4 a,b,c	0.1	0.9	0,0.5,0.99	+3dB	+3dB
5 a,b,c	0.999	0.999	0,0.5,0.99	+3dB	+3dB

Table 1 Signal Process Parameters used in the detection results for Figs. 4 and 5.

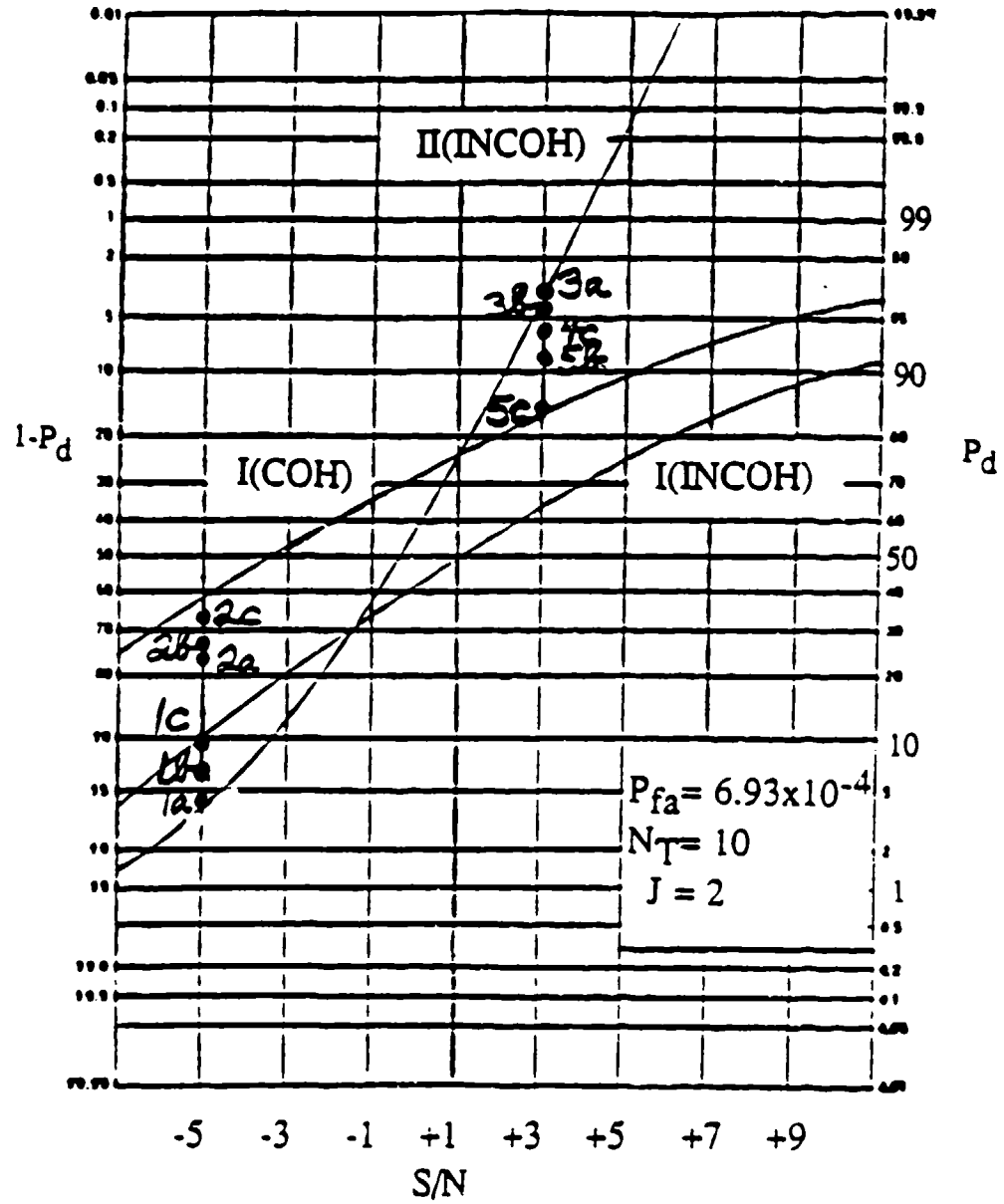

Fig. 4 Probability of detection versus S/N for a Gaussian signal plus Gaussian white noise 'with' F_1 filter coefficients; $S/N=(S/N)_1=(S/N)_2$, $P_{fa}=6.93\times10^{-4}$, N=10, J=2.

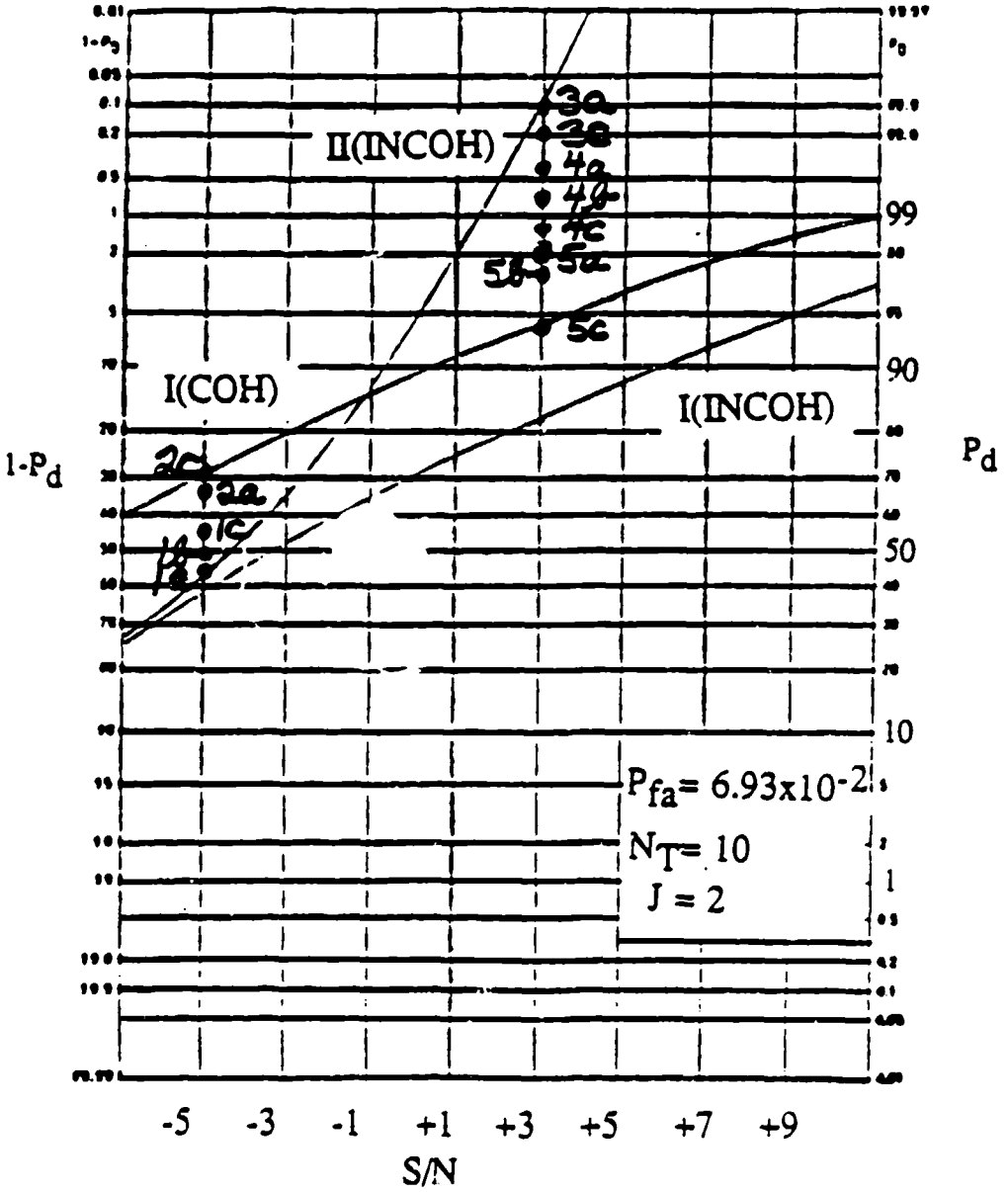

Fig. 5 Probability of detection versus S/N for a Gaussian signal plus Gaussian white noise 'with' F_1 filter coefficients; $S/N=(S/N)_1=(S/N)_2$, $P_{fa}=0.0693$, N=10, J=2.

JN_T=20. In order to compare detection performance for incoherent integration to that of coherent integration, the filter coefficients of the prediction error filters F_0 and F_1 are disabled; ie., the filter coefficients are set to null matrices and the observation data is allowed to pass through the filters unaltered. In this case, the error variances are replaced with the variances of the observation processes under the respective hypotheses. We note that the simulated detection results now range between the model I(INCOH) and model II(INCOH) curves. Consistent with the cross-over of the analytic curves shown in Figs. 4, note that the relative detection performance has reversed for the signal fluctuation models; ie., for the lower S/N value of -5dB, the more highly correlated process of case 2c has a higher P_d than the uncorrelated process of case 1a. Whereas at the higher S/N value of +3dB, the more highly correlated process of case 5c has a lower P_d than the corresponding process of case 3a.

For Figs. 6 through 18, all parameter estimates were obtained using N_{RC}=1 block realization consisting of N_{TC} time samples. The estimates of the filter coefficients for F_0 and F_1 were obtained using observation data from a 'reference' and 'test' cell, respectively.

In Figs. 6 and 7, we plot the probability of detection versus the number of time samples N_{TC} per block for the Gaussian signal in additive Gaussian white noise problem. A signal-to-noise $(S/N)_j$ ratio of 3dB was used on each channel. Each of the three detection curves represents a specific case of signal temporal and cross-channel correlation as designated in the figures. Similar detection plots are shown in Figs 8 and 9 for $(S/N)_j$ = -5dB on each channel. Finally, it is noted that the detection results of Figs. 6 through 9 at N_{TC} = 10,000 are bounded by the analytic detection curves of Figs. 4 and 5 representing the extremes in signal correlation (temporal and cross-channel). Thus, the detection results are shown to converge to those of optimal performance as the parameter estimates improve with increasing sample window sizes.

For the remainder of the detection results presented in this report, we include the presence of Gaussian non-white clutter noise. In Figs. 10 and 11, we plot the computed detection results as a function of the signal-to-noise ratio $(S/N)_j$. For these results, $(S/N)_j$ and $(C/N)_j$ are equal on each channel with

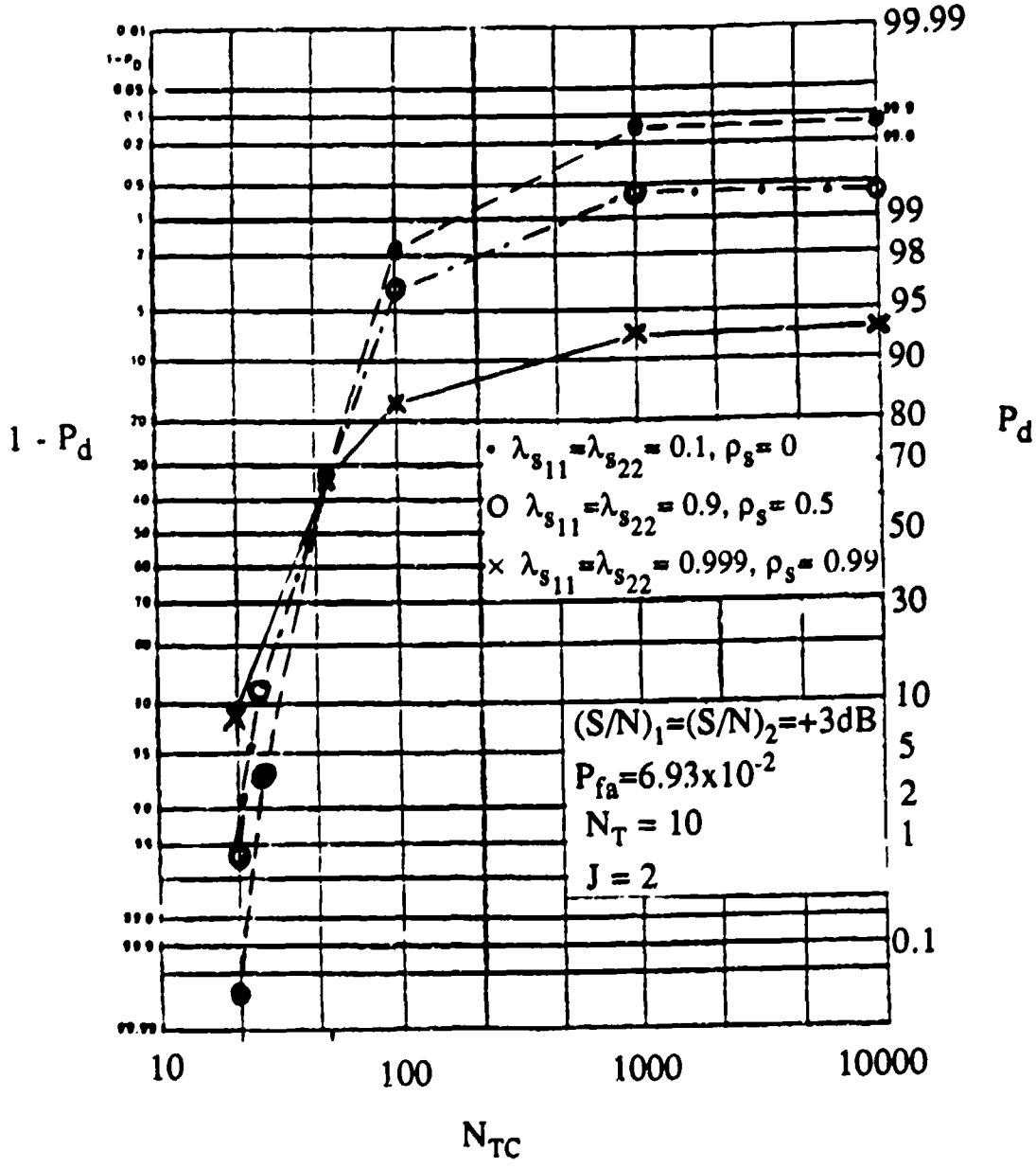

Fig. 6 Probability of detection versus the number of block samples N_{TC} used in parameter estimation via the Strand-Nuttall algorithm for a Gaussian signal in white Gaussian noise; $P_{fa}=6.93\times10^{-2}$, $(S/N)_1=(S/N)_2=+3dB$, $N_T=10$, $J=2$, channel j signal temporal correlation parameter $\lambda_{s_{jj}}$ and signal cross-correlation parameter ρ_s.

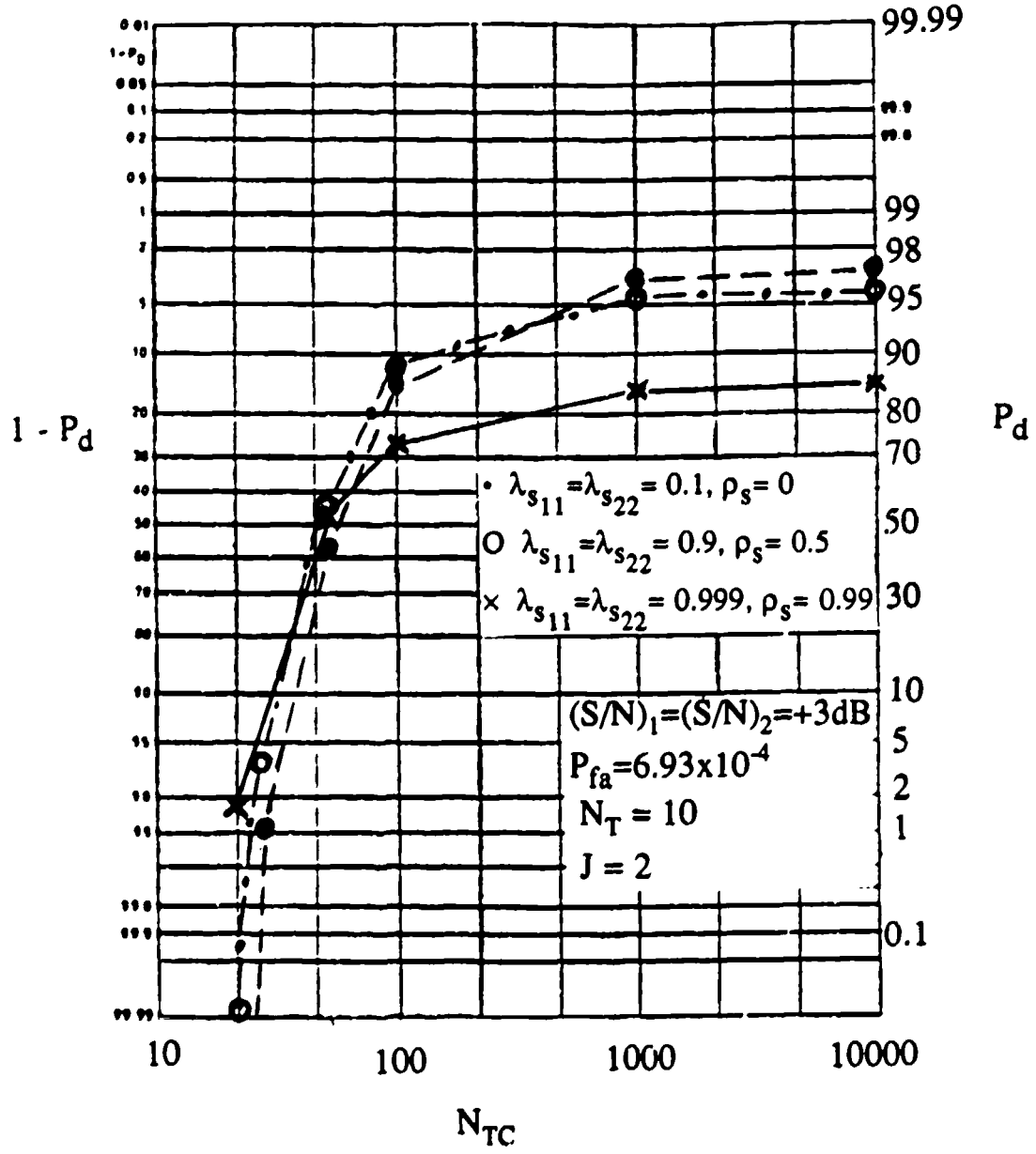

Fig. 7 Probability of detection versus the number of block samples N_{TC} used in parameter estimation via the Strand-Nuttall algorithm for a Gaussian signal in white Gaussian noise; $P_{fa}=6.93\times10^{-4}$, $(S/N)_1=(S/N)_2$=+3dB, N_T=10, J=2, channel j signal temporal correlation parameter $\lambda_{s_{jj}}$ and signal cross-correlation parameter ρ_s.

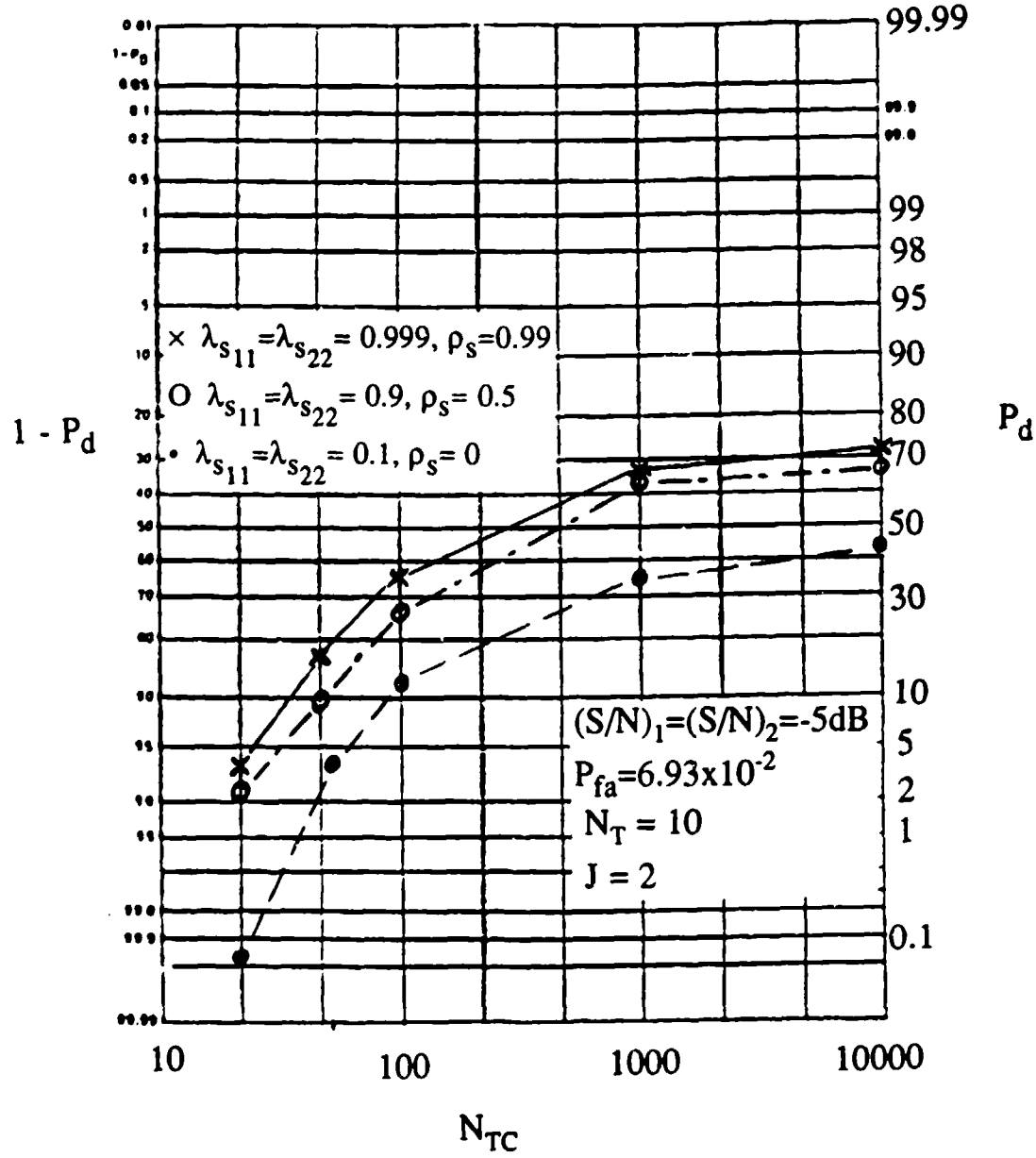

Fig. 8 Probability of detection versus the number of block samples N_{TC} used in parameter estimation via the Strand-Nuttall algorithm for a Gaussian signal in white Gaussian noise; $P_{fa}=6.93x10^{-2}$, $(S/N)_1=(S/N)_2$=-5dB, N_T=10, J=2; channel j signal temporal correlation parameter $\lambda_{s_{jj}}$ and signal cross-correlation parameter ρ_s.

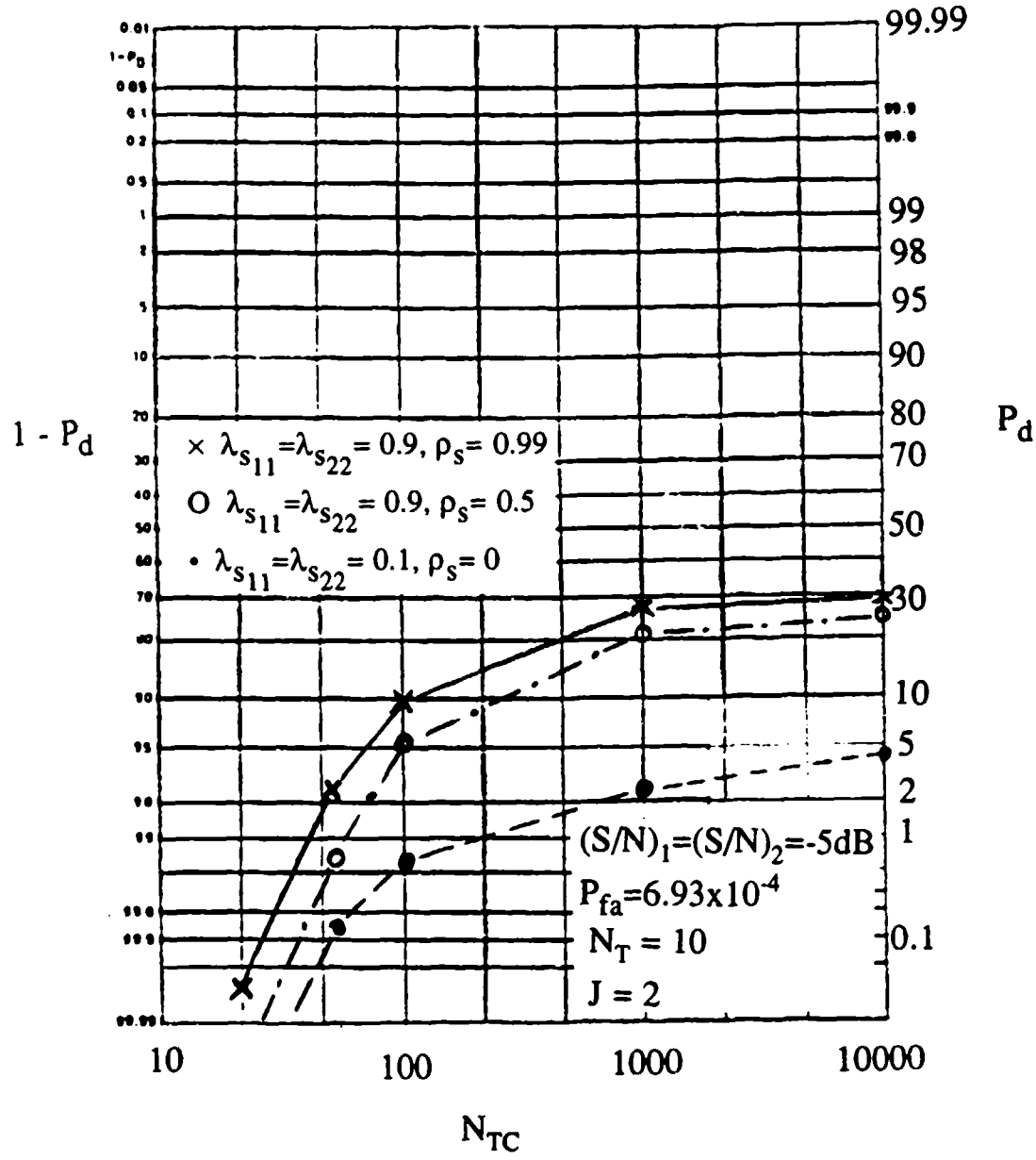

Fig. 9 Probability of detection versus the number of block samples N_{TC} used in parameter estimation via the Strand-Nuttall algorithm for a Gaussian signal in white Gaussian noise; $P_{fa}=6.93x10^{-4}$, $(S/N)_1=(S/N)_2$=-5dB, N_T=10, J=2, channel j signal temporal correlation parameter $\lambda_{s_{jj}}$ and signal cross-correlation parameter ρ_s.

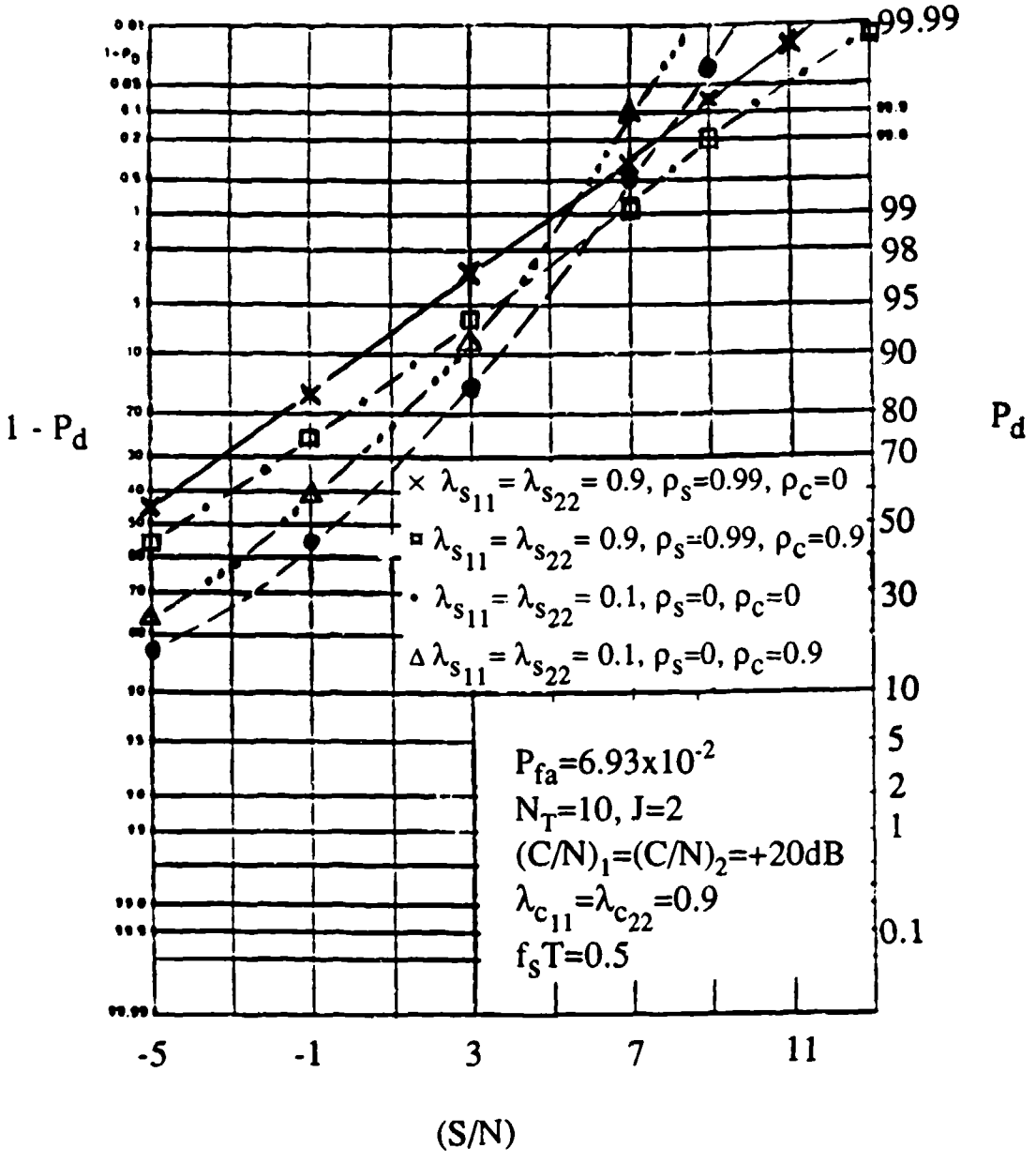

Fig. 10 Probability of detection versus (S/N) for a Gaussian signal in additive Gaussian clutter plus white noise; $P_{fa}=6.93\times10^{-2}$, $(S/N)=(S/N)_1=(S/N)_2$, J=2, $N_T=10$, channel j signal and clutter temporal correlation parameters $\lambda_{s_{jj}}$ and $\lambda_{c_{jj}}$, signal and clutter cross-correlation parameters ρ_s and ρ_c, respectively.

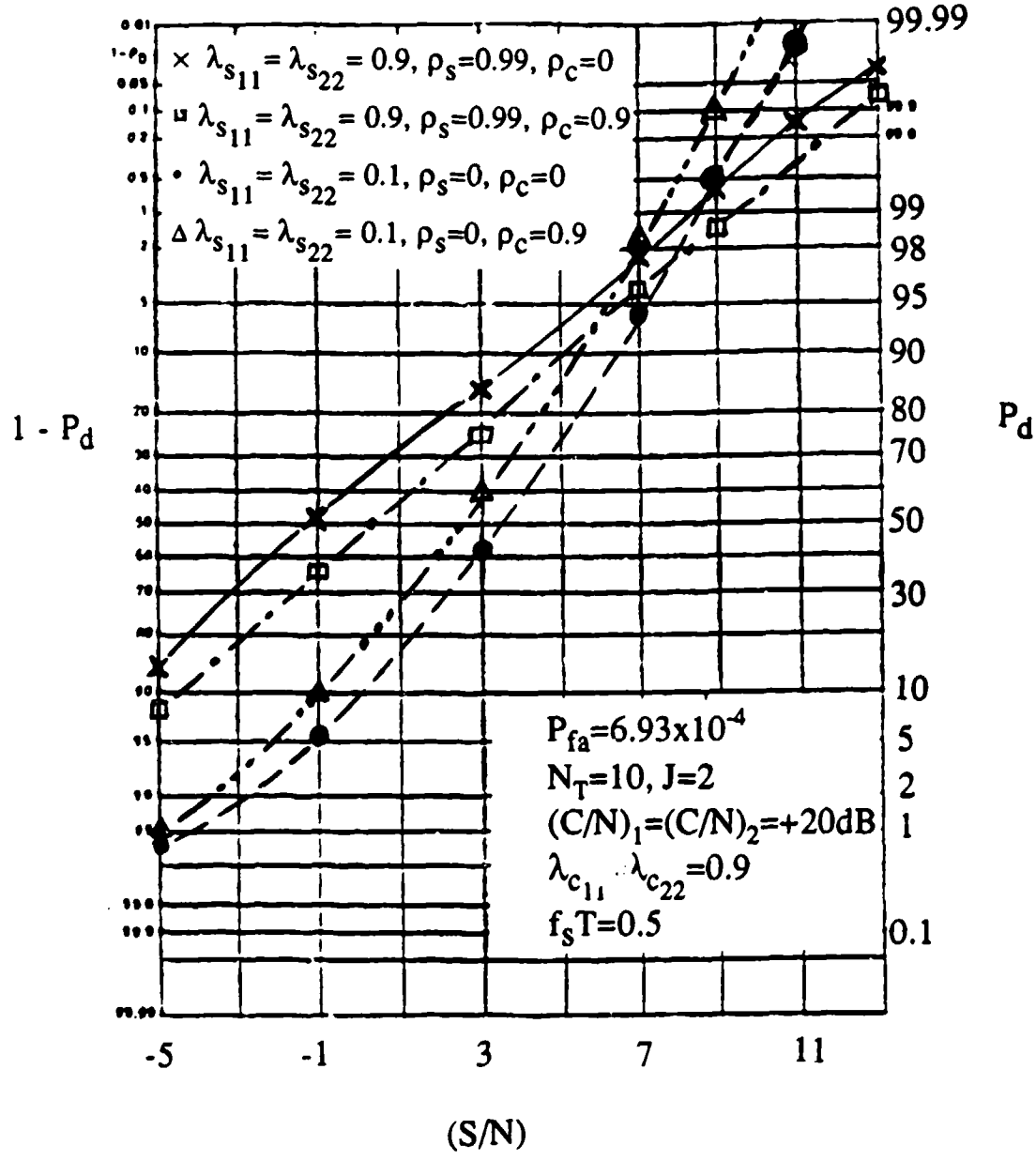

Fig. 11 Probability of detection versus (S/N) for a Gaussian signal in additive Gaussian clutter plus white noise; $P_{fa}=6.93\times10^{-4}$, $(S/N)=(S/N)_1=(S/N)_2$, $J=2$, $N_T=10$, channel j signal and clutter temporal correlation parameters $\lambda_{s_{jj}}$ and $\lambda_{c_{jj}}$, signal and clutter cross-correlation parameters ρ_s and ρ_c, respectively.

$(C/N)_j$ fixed at 20dB. The normalized reference† doppler frequency [7,9] to pulse repetition frequency (PRF) ratio also expressed as f_sT and f_cT for the signal and clutter, respectively, was $f_sT=0.5$ and $f_cT=0$ where T is the sample period (1/PRF). Two sets of clutter cross-correlation parameters were used with $|\rho_{c_{12}}|=0$ and $|\rho_{c_{12}}|=0.9$ to illustrate the effect of increasing cross-channel clutter correlation. The temporal auto-correlation parameter for the clutter was $\lambda_{c_{ii}}=0.9$, i=1,2.

In Figs. 12 through 18, we again consider the probability of detection as a function of the number of block samples N_{TC} used in parameter estimation for processes containing clutter noise. Figs. 12 and 13 show the results for processes with a signal-to-noise (S/N)=3dB on each channel for P_{fa} values $6.93\text{x}10^{-2}$ and $6.93\text{x}10^{-4}$, respectively. Various signal correlation parameters are considered in each of these figures. Also, two cases of clutter temporal correlation with parameters $\lambda_{c_{ii}}=0.9$ and 0.7, i=1,2 both with $\lambda_{c_{12}}=0.1$ are shown in the upper and lower group of curves, respectively. The latter case represents an increase in the spectral spread of the clutter thus increasing the interference with the signal. In Fig. 14, we present the corresponding detection results for the case where (S/N)=-5dB on each channel with $\lambda_{c_{ii}}=0.9$, i=1,2. In this plot, the curves for both P_{fa} values are displayed.

Figs. 15 and 16 show the detection results for the slow fluctuating signal case where again the clutter spectrum has different spectral widths; ie., the upper curves have a temporal correlation parameter $\lambda_{c_{ii}}=0.9$ on both channels whereas the lower curves have $\lambda_{c_{ii}}=0.7$ on both channels. As noted above, the latter case represents an increase in the spectral spread of the clutter which interferes more strongly with the signal thus causing the decrease in P_d. The center curve, however, has $\lambda_{c_{11}}=0.9$ and $\lambda_{c_{22}}=0.7$; ie., the clutter spectrum on channel 2 interferes with the signal more than that on channel 1 due to its larger spectral spread.

Fig. 17 shows the detection results versus N_{TC} for variations in the cross-channel correlation of the clutter at $P_{fa}=6.93\text{x}10^{-4}$. For these results, the more slowly fluctuating signal model with high cross-channel signal correlation (i.e.,

† A reference doppler frequency must be considered in the multichannel case as noted in chapter 2 and is discussed more thoroughly in [10].

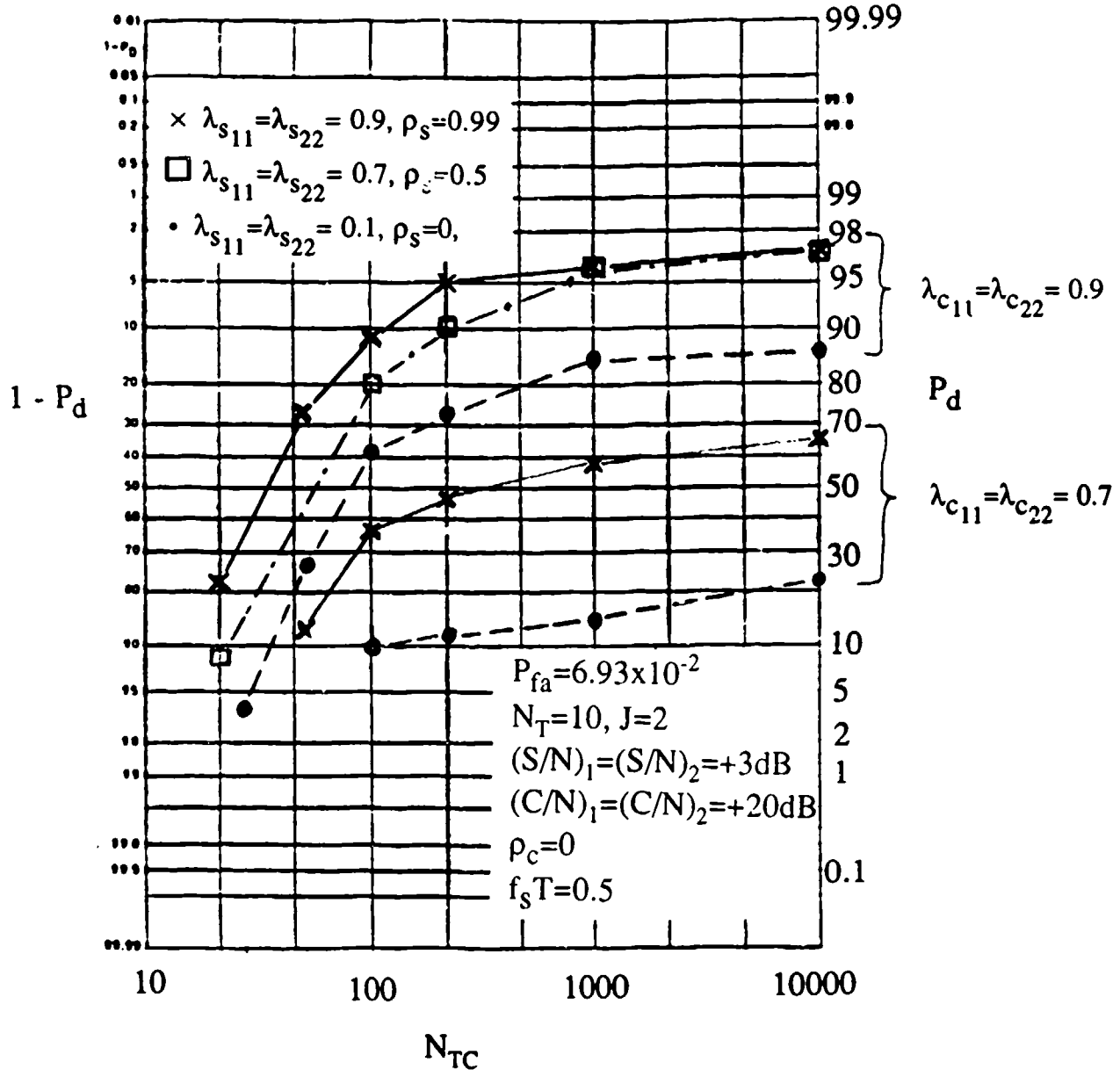

Fig. 12 Probability of detection versus the number of block samples N_{TC} used in parameter estimation via the Strand-Nuttall algorithm for a Gaussian signal in additive Gaussian clutter plus white noise; $P_{fa}=6.93\times10^{-2}$, J=2, N_T=10, channel j signal and clutter temporal correlation parameters $\lambda_{s_{jj}}$ and $\lambda_{c_{jj}}$, signal and clutter cross-correlation parameters ρ_s and ρ_c, respectively.

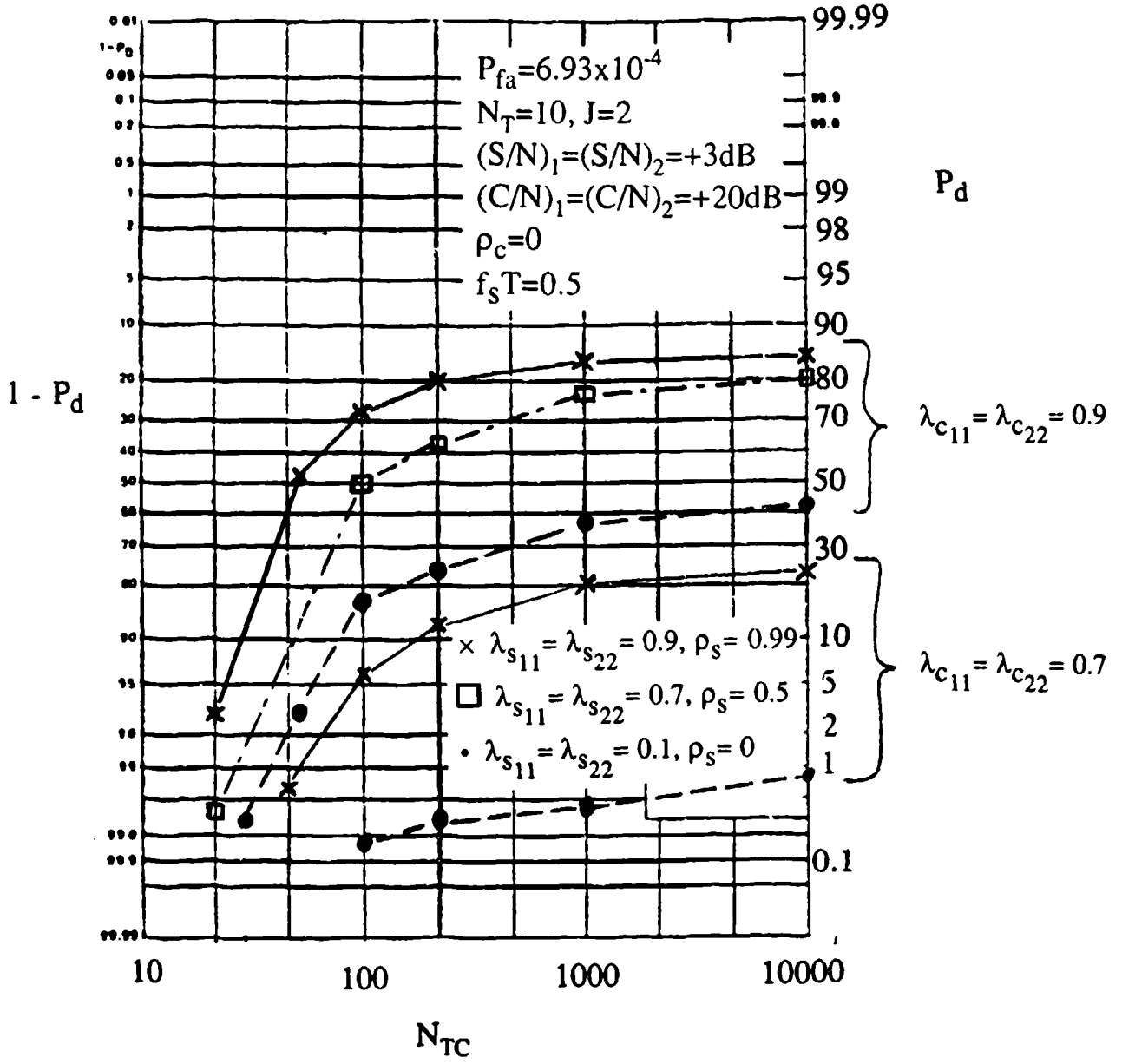

Fig. 13 Probability of detection versus the number of block samples N_{TC} used in parameter estimation via the Strand-Nuttall algorithm for a Gaussian signal in additive Gaussian clutter plus white noise; $P_{fa}=6.93x10^{-4}$, J=2, $N_T=10$, channel j signal and clutter temporal correlation parameters $\lambda_{s_{jj}}$ and $\lambda_{c_{jj}}$, signal and clutter cross-correlation parameters ρ_s and ρ_c, respectively.

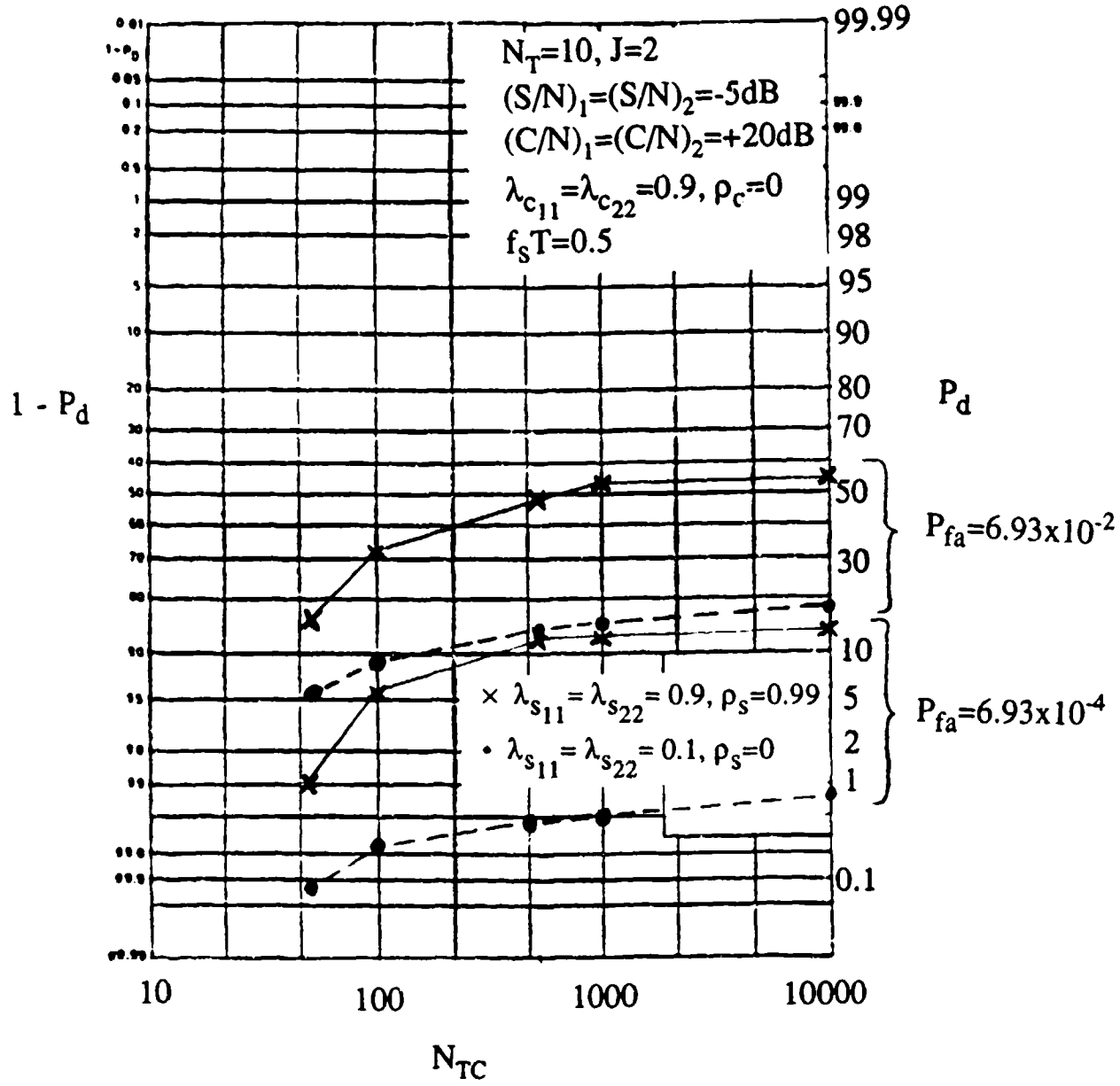

Fig. 14 Probability of detection versus the number of block samples N_{TC} used in parameter estimation via the Strand-Nuttall algorithm for a Gaussian signal in additive Gaussian clutter plus white noise; J=2, N_T=10, channel j signal and clutter temporal correlation parameters $\lambda_{s_{jj}}$ and $\lambda_{c_{jj}}$, and signal and clutter cross-correlation parameter ρ_s and ρ_c, respectively.

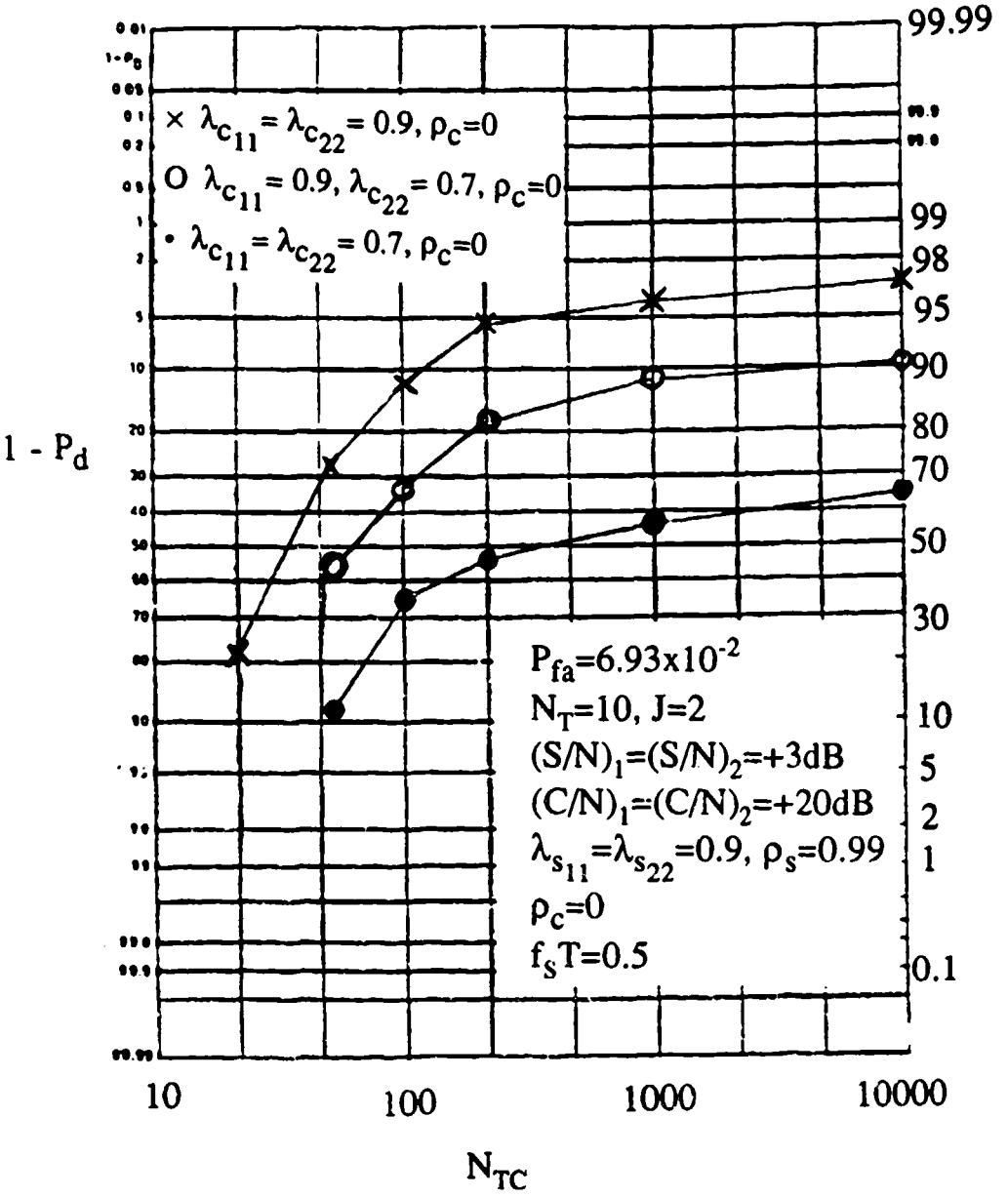

Fig. 15 Probability of detection versus the number of block samples N_{TC} used in parameter estimation via the Strand-Nuttall algorithm for a Gaussian signal in additive Gaussian clutter plus white noise; $P_{fa} = 6.93 \times 10^{-2}$, J=2, $N_T = 10$, channel j signal and clutter temporal correlation parameters $\lambda_{s_{jj}}$ and $\lambda_{c_{jj}}$, signal and clutter cross-correlation parameters ρ_s and ρ_c, respectively.

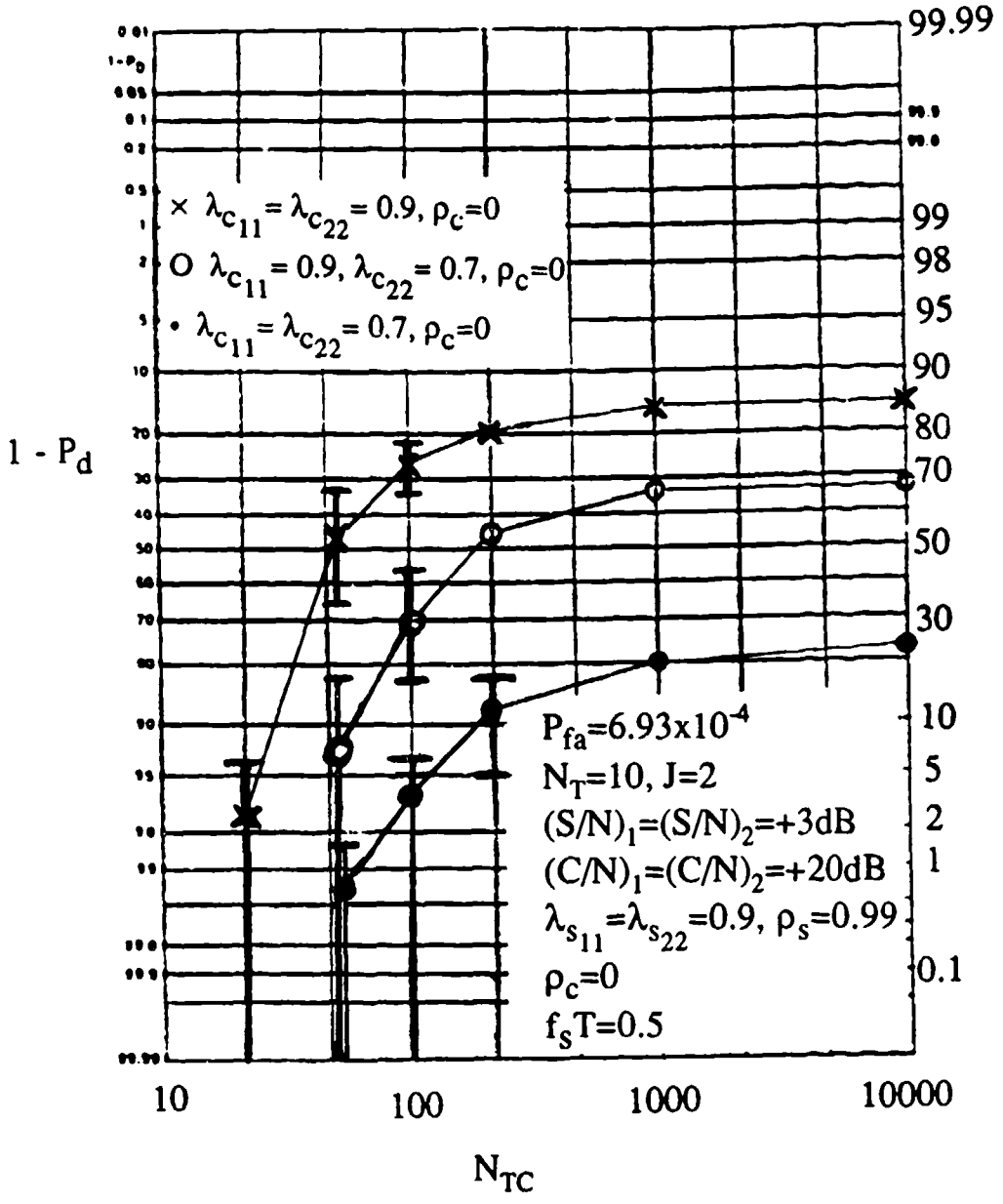

Fig. 16 Probability of detection versus the number of block samples N_{TC} used in parameter estimation via the Strand-Nuttall algorithm for a Gaussian signal in additive Gaussian clutter plus white noise; $P_{fa}=6.93\times10^{-4}$, J=2, $N_T=10$, channel j signal and clutter temporal correlation parameters $\lambda_{s_{jj}}$ and $\lambda_{c_{jj}}$, signal and clutter cross-correlation parameters ρ_s and ρ_c, respectively.

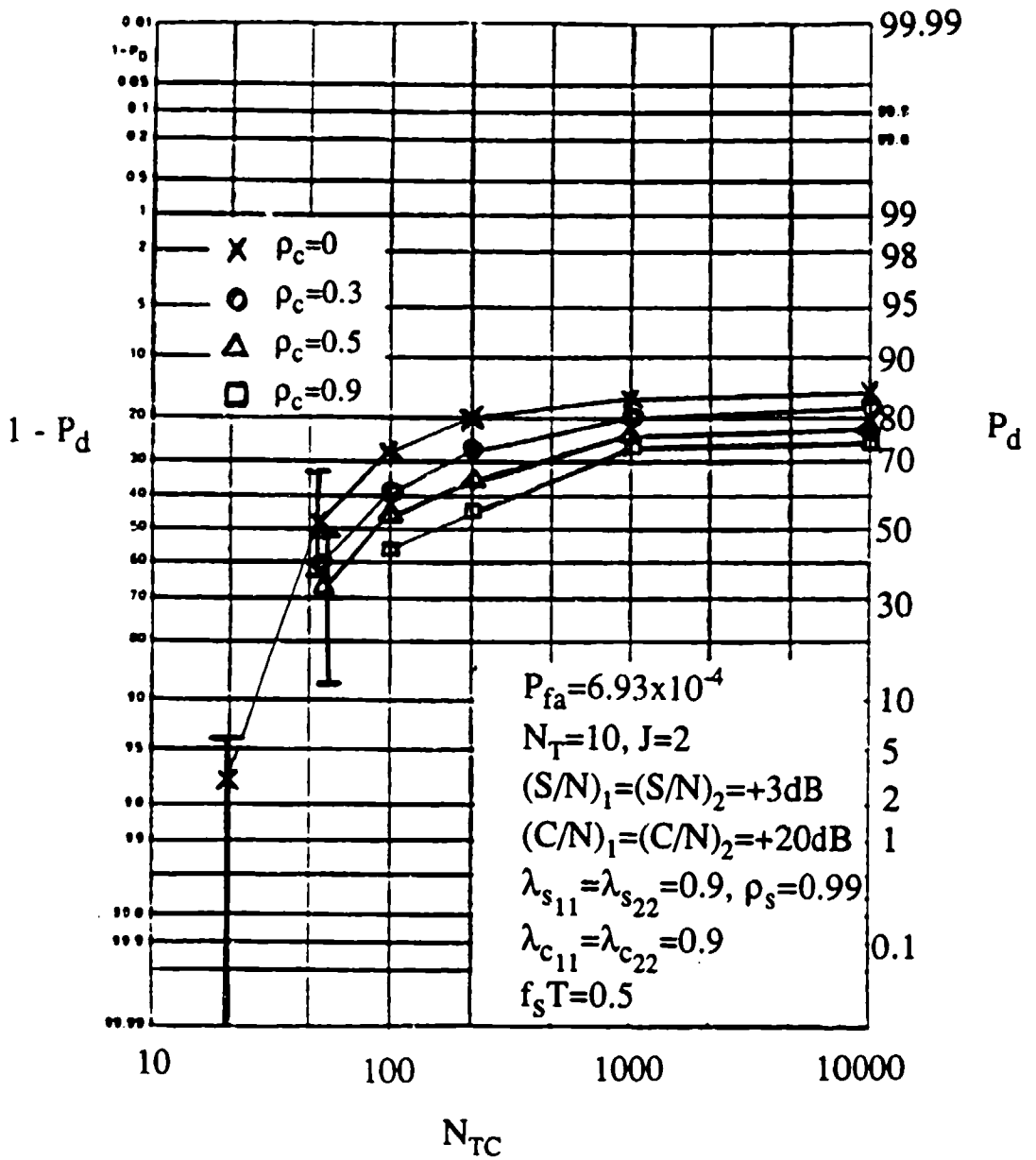

Fig. 17 Probability of detection versus the number of block samples N_{TC} used in parameter estimation via the Strand-Nuttall algorithm for a Gaussian signal in additive Gaussian clutter plus white noise; $P_{fa}=6.93\times10^{-4}$, J=2, N_T=10, channel j signal and clutter temporal correlation parameters $\lambda_{s_{jj}}$ and $\lambda_{c_{jj}}$, signal and clutter cross-correlation parameters ρ_s and ρ_c, respectively.

with $\lambda_{s_{ii}}$=0.9, i=1,2 and $|\rho_s|$=0.99) was used. Signal and clutter-to-noise ratios of (S/N)=3dB and (C/N)=20dB were used on each channel. The results reveal a decrease in probability of detection with increasing cross-channel clutter correlation for the more slowly fluctuating signal model and the specific detection parameters considered in this case. We note that the results shown here labeled X and □ at large N_{TC} (ie., N_{TC} =10,000) are consistent with those shown in Fig. 11 at (S/N)=+3dB. In Fig. 18, however, the signal cross-channel correlation is varied for the more slowly fluctuating signal model ($\lambda_{s_{ii}}$=0.9, i=1,2) while the clutter correlation is held fixed with $\lambda_{c_{ii}}$=0.9 and $|\rho_c|$=0. These results reveal a decrease in probability of detection with decreasing cross-channel signal correlation.

Finally, in Figs. 19 and 20, we consider the case in which one of the channels contains a lower signal-to-noise ratio than the other channel. For these results, $(S/N)_1$=+3dB on channel 1, $(S/N)_2$ on channel 2 ranges from +3dB to -40dB and $\lambda_{s_{11}}=\lambda_{s_{22}}$=0.1 (a fast fluctuating signal). The detection results are also displayed for signal cross-channel correlation coefficients $|\rho_{12}|$=0, 0.5, and 0.99. We also show the P_d value for channel 1 alone using N_T=10. This last result provides the basis for a comparison between the multichannel detection results using $(S/N)_2 < (S/N)_1$ and the results obtained with the superior channel 1 alone. Additional plots are considered in [7].

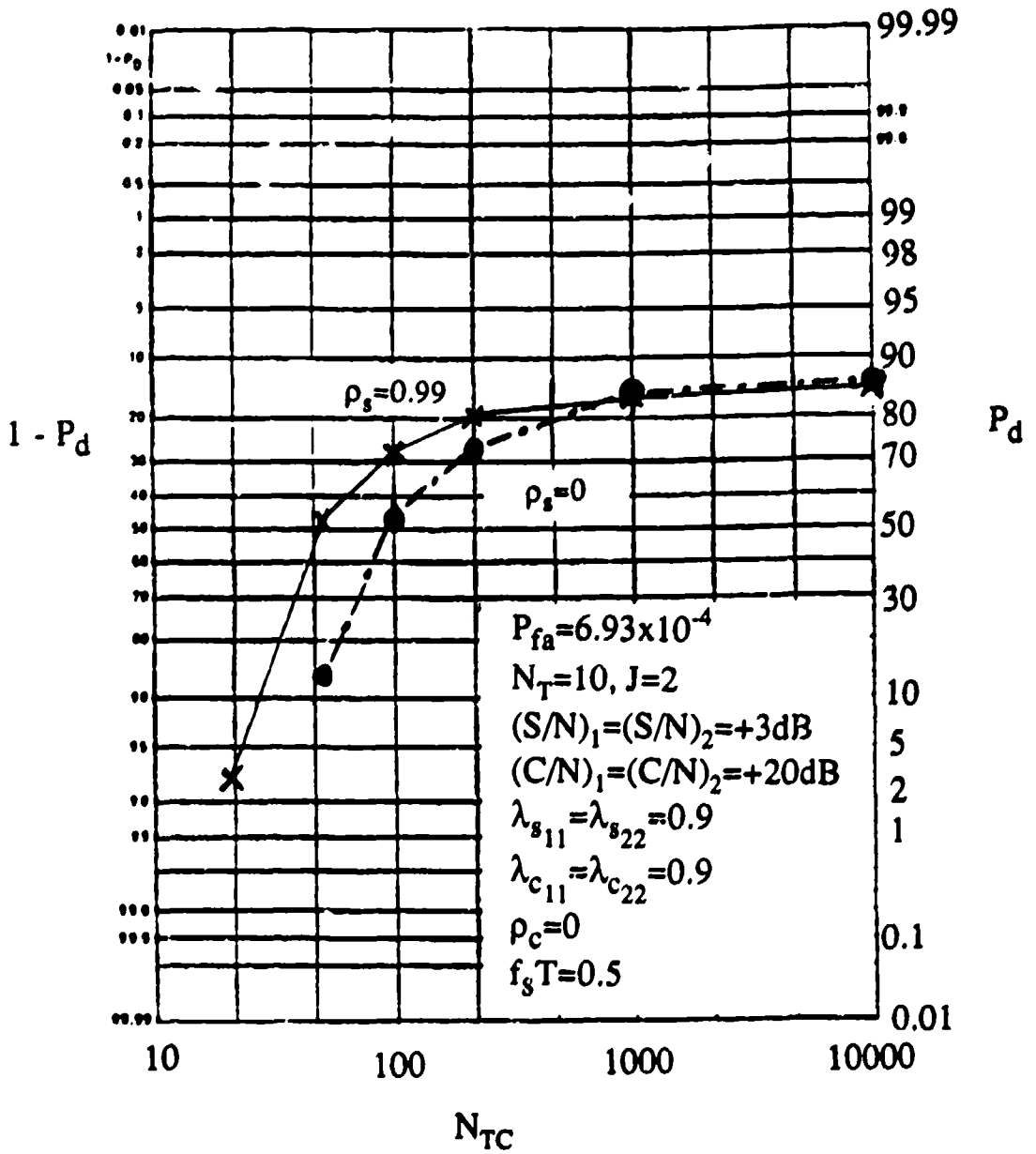

Fig. 18 Probability of detection versus the number of block samples N_{TC} used in parameter estimation via the Strand-Nuttall algorithm for a Gaussian signal in additive Gaussian clutter plus white noise; $P_{fa}=6.93\times10^{-4}$, J=2, N_T=10, channel j signal and clutter temporal correlation parameters $\lambda_{s_{jj}}$ and $\lambda_{c_{jj}}$, signal and clutter cross-correlation parameters ρ_s and ρ_c, respectively.

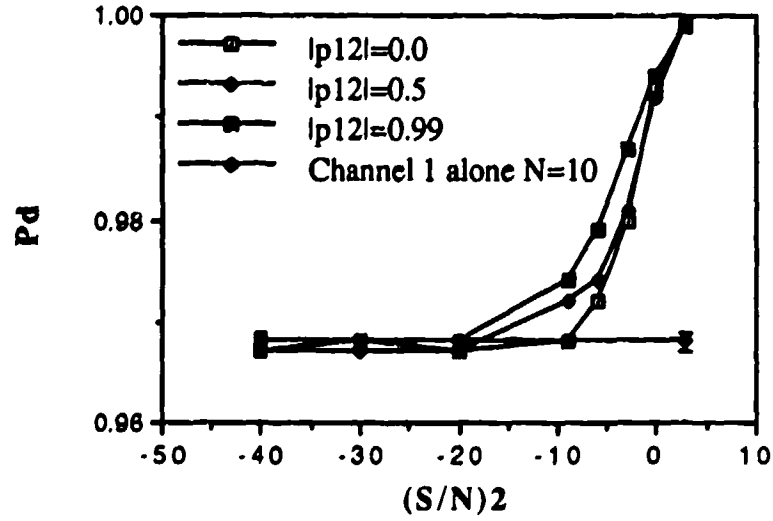

Figure 19 Two channel probability of detection results as a function of $(S/N)_2$ and $|\rho_{12}|$ for P_{fa}= 0.0693, $(S/N)_1$=+3dB and $\lambda_{11}=\lambda_{22}=0.1$.

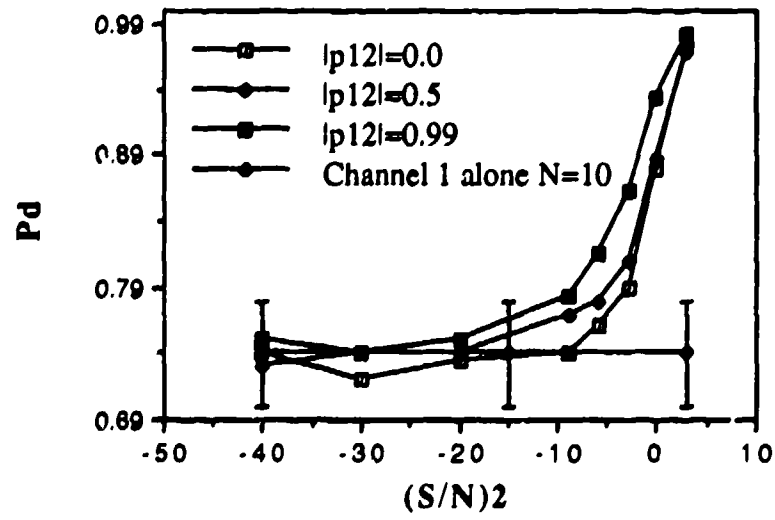

Figure 20 Two channel probability of detection results as a function of $(S/N)_2$ and $|\rho_{12}|$ for $P_{fa}=6.93\times10^{-4}$, $(S/N)_1$=+3dB and $\lambda_{11}=\lambda_{22}=0.1$.

CHAPTER 6 DISCUSSION OF RESULTS

Inspection of the detection curves contained in this report reveals several interesting features. First, in Figs. 4, 5, 10 and 11, we note the cross-over point between the fast-fluctuating and slow-fluctuating signal detection curves. For these detection results, the estimators used in the filters F_0 and F_1 have reached their steady-state values after processing N_{TC}=10,000 time samples. In Fig. 5, for example, the model I(COH) and model II(INCOH) curves intersect at S/N= +1dB. In this case, we have considered the Gaussian signal in additive white Gaussian noise. We have purposely selected processes with S/N values above and below these intersection points in order to investigate the effect of the temporal and cross-channel correlation on detection performance in both regions. We anticipate that processes uncorrelated both temporally and across channels will lie closer to the model II(INCOH) bound while those with high correlation will lie closer to the model I(COH) bound. Thus, the effect of the temporal and cross-channel correlation for both the signal and clutter on the detection results is dependent upon the location along the detection curve with respect to this cross-over point; ie., at (S/N) values above this point, the fast-fluctuating signal model provides the superior performance whereas at (S/N) values below it, the slow-fluctuating signal model dominates. Furthermore, the presence of the non-white clutter process also effects the position of this cross-over point. Specifically, in Fig. 11, where the processes have a clutter-to-noise ratio of 20dB on each channel, we note that the cross-over point for the processes with high cross-channel clutter correlation occurs at (S/N)=+6dB as compared to +9dB when no cross-channel correlation is present. In general, the cross-over point for the detection curves is a function of the temporal and cross-channel correlation of both the signal and clutter processes as well as parameters such as $(C/N)_j$, P_{fa} and N_T. We also note that for the cases with high cross-channel clutter correlation (ie., $|\rho_{c_{12}}|$=0.9), the increasing cross-channel correlation causes a decrease in P_d for the more slowly fluctuating signal ($\lambda_{s_{ii}}$=0.9, i=1,2), but an increase for the fast-fluctuating signal ($\lambda_{s_{ii}}$=0.1, i=1,2). These results can be explained by noting that the increased cross-channel clutter correlation can be used to discriminate the fast fluctuating signal from the clutter more readily than the more slowly fluctuating signal. Finally, we point out that for the results shown in Figs. 10 and 11, the slow fluctuating signal model provides the higher performance results for

(S/N) below values in the 4 to 9dB cross-over range. Thus, at the (S/N) values of -5dB and +3dB which are primarily considered in this report, the slow-fluctuating signal case in the presence of clutter provides the superior detection performance over the fast-fluctuating case.

Next, we consider the 'transient' condition in which the estimators have not reached their 'steady-state' values due to limited data sample sizes used in the estimation procedure. The detection results in Figs. 6 through 9 for the various signal fluctuation models in additive white noise, asymptotically approach those shown in Figs. 4 and 5 and are bounded by the analytic detection curves representing the extremes in signal correlation (temporal and cross-channel). Furthermore, they are consistent with the detection performance reversal about the cross-over point as described above. Thus, as the estimators approach steady-state for large N_{TC}, the detection results are shown to converge to their optimal values. Likewise, the detection values shown in Figs 12 through 18 asymptotically approach those shown in Figs. 10 and 11. Analytic detection curves for the latter will be reported in future investigations involving partially correlated clutter processes.

Examination of Figs. 12 and 13 indicates that as the temporal correlation of the clutter decreases from $\lambda_{c_{ii}}=0.9$ to $\lambda_{c_{ii}}=0.7$, i=1,2 the detection performance decreases significantly. This result is to be expected since the decrease in the temporal correlation of the clutter causes an increase in its spectral width on both channels. Thus, the clutter interferes more strongly with the signal at its normalized Doppler location of $f_sT=0.5$ in the frequency spectrum.

The detection performance shown on the the center curve of Figs. 15 and 16 with $\lambda_{c_{11}}=0.9$ on channel 1 and $\lambda_{c_{22}}=0.7$ on channel 2 describes the situation where the signal on channel 1 is less affected by the narrower clutter noise spectrum than that on channel 2. The detection results for this case show that a significant improvement in detection performance can be obtained for the case where one of the two channels operates 'in the clear' as compared to the case where both channels have high interference.

An interesting feature associated with the performance of the parameter estimation procedure can be observed in several of the results. In Figs. 6 through 9 and 12 through 18, we observe that the rate at which the detection curves approach their asymptotic values for increasing N_{TC} is significantly affected not only by $(S/N)_j$ and $(C/N)_j$, but also by the process correlation. In the next several cases, we observe that increases in the temporal correlation of the data processes provide a faster convergence rate to the asymptotic detection values.

In Figs. 6 and 7, we consider the Gaussian signal in additive Gaussian white noise problem for $(S/N)_j$=+3dB on each channel. At this $(S/N)_j$ value, the detection performance for the fast-fluctuating signal model is higher than that for the slow-fluctuating model when the estimators have reached their steady-state values using high values of N_{TC}. This is verified by observing the results shown in Figs. 4 and 5 which describe the 'steady-state' case. Thus, for N_{TC}>50, the superior detection performance associated with the fast fluctuating signal model at this (S/N) value dominates the results as expected. However, for N_{TC}<50, we note that the superior performance is obtained for the slow-fluctuating (more highly correlated) signal model.

In Fig. 13, for the upper three curves with temporal clutter correlation parameters $\lambda_{c_{11}}=\lambda_{c_{22}}=0.9$, we note that the probability of detection reaches within 4% of its asymptotic value at N_{TC}=200 for signal processes with high temporal and cross-channel correlation ($\lambda_{s_{jj}}=0.9$). However, for signal processes with low temporal correlation ($\lambda_{s_{jj}}=0.1$), these levels are not achieved until N_{TC}=1,000. For the lower curves, however, where $\lambda_{c_{11}}=\lambda_{c_{22}}=0.7$, P_d is only within 50% of its asymptotic value at N_{TC}=200 as compared to the 4% value noted above.

In Fig. 16, we also note that the convergence rate for the upper curve (with high clutter temporal correlation on both channels) is significantly faster than that for the lower curve (with lower temporal clutter correlation); ie., the upper curve is within 5% of its asymptotic value at N_{TC}=200 whereas the lower curve is only within 50% at this value.

In Figs. 17 and 18, we observe the effect of the process cross-correlation on the convergence rates. Fig. 17 shows the detection results versus N_{TC} for variations in the cross-channel correlation of the clutter. For these results, the more slowly fluctuating signal model was used with $\lambda_{s_{jj}}=0.9$, j=1,2 and $|\rho_{s_{12}}|=0.99$. Signal and clutter-to-noise ratios of (S/N)=3dB and (C/N)=20dB, respectively, were used on each channel. With the parameters considered here and the more slowly fluctuating signal model, the results reveal a decrease in probability of detection with increasing cross-channel clutter correlation. These results are consistent with those shown in Fig. 11. We note from the two lower curves at (S/N)=3dB in Fig.11, however, that the opposite trend is obtained for the fast fluctuating signal model; i.e., P_d increases with increasing cross-channel clutter correlation. We also note in Fig. 17, that the convergence rate of the

detection performance is superior for the case of no cross-channel correlation; ie., for $|\rho_c|=0$, the detection probability is within 5% of the steady-state value at $N_{TC}= 200$, whereas for $|\rho_c|=0.9$, $N_{TC}\geq 1{,}000$ is required. In Fig. 18, however, the signal cross-channel correlation is varied while the clutter correlation is held fixed with $\lambda_{c_{ii}}=0.9$ and $|\rho_c|=0$. These results reveal a decrease in probability of detection with decreacing cross-channel signal correlation. It also appears that the convergence rate has increased slightly for the case where $|\rho_s|=0.99$. Further consideration of these observations will be made in forthcoming analyses.

The dependence of detection performance on N_{TC} noted in the above results is attributed to the fact that the error variance associated with the multichannel parameter estimators is directly related to both the temporal and cross-channel correlation of the processes as well as the data sample window size, N_{TC} [15]. The interesting result noted in [15] is that, unlike the estimators for covariance matrices, the error variance of parameter estimators, such as that considered here, decreases with increasing temporal correlation. Thus, the detection performance resulting when limited data is used is dependent upon the signal and clutter correlation both directly as well as indirectly through dependence upon the performance of the estimation procedure. In some cases, this direct and indirect dependence may be inversely related as noted in Figs 6 and 7. In these figures, the superior performance of the estimator using the more correlated processes dominates with limited data (N_{TC} small) whereas with larger data window sizes (N_{TC} large), the detection performance is dependent upon the process correlation only.

In the previously results, we considered the situation in which $(S/N)_j$ was the same on both channels. In Figs. 19 and 20, we consider the situation in which $(S/N)_j$ remains the same on one channel but is lowered on the other channel. In this case, the overall detection performance will degrade from the previous cases. For the results shown here, $(S/N)_1$ was held fixed at +3dB while $(S/N)_2$ was varied from +3dB to -40dB. In each case, two channels each with ten observations were considered (ie., J=2 and N_T=10). Again, we note that no cross-channel correlation is considered on the noise processes. The coherent detection results are shown in Figs. 19 and 20 for $P_{fa}=0.0693$ and $6.93\text{x}10^{-4}$, respectively, with signal one-lag temporal correlation parameters $\lambda_{11}=\lambda_{22}=0.1$. The values are also displayed for signal cross-channel correlation coefficients $|\rho_{12}|=0$, 0.5, and 0.99. We also show the P_d value for channel 1 alone using

N_T=10. This last result provides the basis for a comparison between the two-channel detection results using $(S/N)_2 < (S/N)_1$ and the results obtained with channel 1 alone. These results indicate that the two-channel case shows improved detection performance over that of the channel 1 case alone. Furthermore, as $(S/N)_2$ decreases, the two-channel detection results for these cases approach that of channel 1 alone. More examples are shown in [7].

CHAPTER 7 CONCLUSIONS

In this report, we have considered the Gaussian multichannel detection problem in which the signal and additive non-white clutter noise have 'unknown' statistics. A multichannel generalized likelihood ratio is implemented using a model-based approach where the signal and clutter are assumed to be characterized by autoregressive (AR) vector processes. In the case considered here, the parameters of the underlying processes are 'unknown' and are estimated using the Stand-Nuttall algorithm (a multichannel generalization of the Burg algorithm). Detection results are obtained for a two-channel detection problem using a Monte-Carlo procedure and performance is assessed as the estimators approach their 'steady-state' values. Furthermore, the convergence rates are considered as a function of the signal and clutter-to-noise ratios as well as the temporal and cross-correlation of the signal and clutter.

REFERENCES

[1] Schweppe, F., "Evaluation of Likelihood Functions for Gaussian Signals," IEEE Trans. IT-11, No. 1,61-70 (Jan 1965).

[2] Therrien, C.W. "A Sequential Approach to Target Discrimination," IEEE Trans. on Aerospace and Electronic Systems, vol AES-14, no.3, pp. 443-440, May 1978.

[3] Farina, A., Russo, A., "Radar detection of correlated targets in clutter," IEEE Trans. on Aerospace and Electronics Systems, vol AES-22, no 5, Sept. 1986.

[4] Haykin, S., Zhang, Q.T. "A model-based detection approach," IEEE Radar Conference, 1986.

[5] Haykin, S., Metford, P.A.S., "Experimental analysis of an innovations-based detection algorithm for surveillance radar," IEE Proc., Vol 132, Pt F, no 1, Feb. 1985.

[6] Metford, P.A.S., Haykin, S., Taylor, D., "An innovations approach to discrete-time detection theory," IEEE Trans. on Information Theory, Vol IT-28, no 2, March 1982.

[7] Michels, J.H., "Multichannel Detection using the Discrete-Time Model-Based Innovations Approach," Ph.D. dissertation, Syracuse University, Syracuse, N.Y., May, 1991.

[8] Michels, J. H., "Synthesis of Multichannel Autoregressive Random Processes and Ergodicity Considerations," RADC-TR-90-211, July, 1990.

[9] Michels, J. H., Varshney, P., Weiner, D., "Synthesis of Correlated Multichannel Random Processes", accepted for publication in the Transactions on Signal Processing.

[10] Meyer, D.P., Mayer, H.A., Radar Target Detection, Handbook of Theory and Practice, Academic Press, New York, 1973.

[11] Strand, O. N., "Multichannel complex maximum entropy (auto-regressive) spectral analysis," IEEE Trans. Antom. Control, vol, AC-22, pg 634-640, Aug 1977.

[12] Nuttall, A.H., "Multivariate linear predictive spectral analysis employing weighted forward and backward averaging: A generalization of Burg's algorithm," Naval Underwater Systems Center TR-5501, New London, Conn. Oct. 1976.

[13] Marple, S. L., Digital Spectral Analysis with Applications, Prentice Hall, N.J., 1987.

[14] Burg, J.P., "Maximum Entropy Spectral Analysis," Ph.D. dissertation, Stanford University, Stanford, California, 1975.

[15] Michels, J.H., "Considerations of the Error Variance of Time-Averaged Estimators for Correlated Processes", to be published as a Rome Laboratory In-House technical report.

[16] Michels, J.H., Varshney, P., Weiner, D., "Multichannel detection using a model-based approach," 1991 International Conference on Acoustics Speech and Signal Processing, May 14-17, 1991, Toronto, Ontario, Canada, pp. 3553-3556.

[17] Michels, J.H., "Detection of Partially Correlated Signals in Clutter', IEEE Proc. of the National Telesystems Conference, Washington D.C., 19-20 May, 1992, pp. 7-1 to 7-8.

•U.S. GOVERNMENT PRINTING OFFICE 1993-[illegible]

MISSION

OF

ROME LABORATORY

Rome Laboratory plans and executes an interdisciplinary program in research, development, test, and technology transition in support of Air Force Command, Control, Communications and Intelligence (C^3I) activities for all Air Force platforms. It also executes selected acquisition programs in several areas of expertise. Technical and engineering support within areas of competence is provided to ESD Program Offices (POs) and other ESD elements to perform effective acquisition of C^3I systems. In addition, Rome Laboratory's technology supports other AFSC Product Divisions, the Air Force user community, and other DOD and non-DOD agencies. Rome Laboratory maintains technical competence and research programs in areas including, but not limited to, communications, command and control, battle management, intelligence information processing, computational sciences and software producibility, wide area surveillance/sensors, signal processing, solid state sciences, photonics, electromagnetic technology, superconductivity, and electronic reliability/maintainability and testability.